

AD-A126 653

TECHNICAL  
LIBRARY

AD

AD-E400 987

TECHNICAL REPORT ARLCD-TR-82026

**CARS SPECTRA  
FROM LEAN AND STOICHIOMETRIC CH(4)-N(2)O FLAMES**

**L. E. HARRIS**

**MARCH 1983**



**US ARMY ARMAMENT RESEARCH AND DEVELOPMENT COMMAND  
LARGE CALIBER  
WEAPON SYSTEMS LABORATORY  
DOVER, NEW JERSEY**

**APPROVED FOR PUBLIC RELEASE; DISTRIBUTION UNLIMITED.**

The views, opinions, and/or findings contained in this report are those of the author(s) and should not be construed as an official Department of the Army position, policy, or decision, unless so designated by other documentation.

The citation in this report of the names of commercial firms or commercially available products or services does not constitute official endorsement by or approval of the U.S. Government.

Destroy this report when no longer needed. Do not return to the originator.

UNCLASSIFIED

SECURITY CLASSIFICATION OF THIS PAGE (When Data Entered)

REPORT DOCUMENTATION PAGE		READ INSTRUCTIONS BEFORE COMPLETING FORM
1. REPORT NUMBER Technical Report ARLCD-TR-82026	2. GOVT ACCESSION NO. -	3. RECIPIENT'S CATALOG NUMBER
4. TITLE (and Subtitle) CARS SPECTRA FROM LEAN AND STOICHIOMETRIC CH(4)-N(2)O FLAMES		5. TYPE OF REPORT & PERIOD COVERED
		6. PERFORMING ORG. REPORT NUMBER
7. AUTHOR(s)  L.E. Harris		8. CONTRACT OR GRANT NUMBER(s)
9. PERFORMING ORGANIZATION NAME AND ADDRESS ARRADCOM, LCWSL Applied Sciences Div (DRDAR-LCA-G) Dover, NJ 07801		10. PROGRAM ELEMENT, PROJECT, TASK AREA & WORK UNIT NUMBERS  IL16122AH60
11. CONTROLLING OFFICE NAME AND ADDRESS ARRADCOM, TSD STINFO Div (DRDAR-TSS) Dover, NJ 07801		12. REPORT DATE March 1983
		13. NUMBER OF PAGES 46
14. MONITORING AGENCY NAME & ADDRESS (if different from Controlling Office)		15. SECURITY CLASS. (of this report)  Unclassified
		15a. DECLASSIFICATION/DOWNGRADING SCHEDULE
16. DISTRIBUTION STATEMENT (of this Report)  Approved for public release; distribution unlimited.		
17. DISTRIBUTION STATEMENT (of the abstract entered in Block 20, if different from Report)		
18. SUPPLEMENTARY NOTES  Portions of this report are extracted from Technical Report ARLCD-TR-82020, "Broadband N(2) and N(2)O CARS Spectra from a CH(4)-N(2)O Flame", December 1982, L.E. Harris.		
19. KEY WORDS (Continue on reverse side if necessary and identify by block number)  Broadband CARS CARS spectra Spectroscopy		
20. ABSTRACT (Continue on reverse side if necessary and identify by block number)  Broadband CARS spectra were obtained from both the reaction zone and post-flame region of lean and stoichiometric CH(4)-N(2)O flames. To assess methods of obtaining concentration from broadband spectra, N(2) CARS spectra were obtained from a series of air and argon (AIR/AR) mixtures at room temperature. The con- centration of N(2) with good accuracy (6%) was obtained both from fitting the shape of the broadband spectra and from the ratio of the resonant to nonresonant susceptibility. Both methods were utilized in interpreting flame spectra. (cont)		

## 20. ABSTRACT (cont)

CARS spectra of both  $N(2)$  and  $N(2)O$  were obtained from the reaction zone of near 0.3 equivalence ratio (fuel/oxidizer)  $CH(4)-N(2)O$  flames. Spectra were obtained from room temperature to near the adiabatic flame temperature. Simultaneous observation of both  $N(2)$  and  $N(2)O$  spectra allows determination of temperature and concentration of both species from the same point in the flame. The spectra demonstrated the high spatial resolution of CARS.

In addition,  $N(2)$  CARS spectra were obtained from the post-flame region of 0.3, 0.4, 0.5 and 1.0  $CH(4)-N(2)O$  flames. The  $N(2)$  spectra were used to obtain concentration and temperature profiles by a least squares fit to model calculations. The temperatures obtained varied with reactant flow rates. However, at appropriate flow rates, the concentrations and temperatures obtained close to the burner surface were in accord with thermochemical calculation.

The temperature and concentration profiles obtained from both  $N(2)$  and  $N(2)O$  CARS spectra can be used to understand the elementary processes occurring in the  $CH(4)-N(2)O$  flames investigated.

## CONTENTS

	Page
Introduction	1
Experimental Method	2
Results	3
Theory	3
Air/Argon Mixtures	4
Reaction Zone Spectra	5
Post-Flame Spectra	6
Discussion	7
References	11
Distribution List	31

## TABLES

	Page
1 Concentration of air (%) in air/ar mixtures at 300 K	13
2 Temperature and concentration in the reaction zone of a $\text{CH}_4\text{-N}_2\text{O}$ flame (2 mm above the burner)	13
3 Thermochemical calculations for $\text{CH}_4\text{-N}_2\text{O}$ flames	14
4 Measured and calculated temperature (K) and $\text{N}_2$ concentration (%) in a $\text{CH}_4\text{-N}_2\text{O}$ flame	14
5 Temperature and $\text{N}_2$ concentration profile in a $\text{CH}_4\text{-N}_2\text{O}$ flame ( $\phi = 0.5$ ) at a flow of 16.9 cm/s (TCALC = 2734K, CCALC = 58%)	15
6 Temperature and $\text{N}_2$ concentration profile in a $\text{CH}_4\text{-N}_2\text{O}$ flame ( $\phi = 0.5$ ) at a flow of 33.4 cm/s (TCALC = 2734K, CCALC = 58%)	15

## FIGURES

1 Nonplanar BOXCARS spectrometer where BS is a 50% beam splitter, M is a Mirror, OF is an optical flat rotatable about its horizontal axis and T is a beam terminator	17
2 Normalized nitrogen CARS spectra from room temperature air/argon mixtures containing 0% to 23% air	18
3 Normalized nitrogen CARS spectra from room temperature air/argon mixtures containing 3% to 100% air	19
4 Experimental (•) and calculated $\text{N}_2$ CARS spectra at room temperature in a 9% air/argon mixture (nonplanar CARS)	20
5 Experimental (•) and calculated $\text{N}_2$ CARS spectra at room temperature in a 20% air/argon mixture (nonplanar CARS)	21
6 Experimental (•) and theoretical $\log(I_{10} - I_{nr})/I_{nr}$ where $I_{10}$ and $I_{nr}$ are the maximum intensities of nitrogen $Q_{10}$ and the nonresonant susceptibility versus $\log[C(\%)]$	22
7 CARS spectra observed 1 mm above the burner head in a 0.27 $\text{CH}_4\text{-N}_2\text{O}$ flame (the distance indicated is from the centerline of the burner)	23

8	CARS spectra observed 1 mm above the burner head in a 0.27 CH <sub>4</sub> -N <sub>2</sub> O flame (•) compared to theoretical spectra (solid line), calculated at T = 800 K and C = 14% N <sub>2</sub> and T = 1200 and C = 20% N <sub>2</sub> for spectra obtained 1.40 (TOP SPECTRUM) and 1.14 mm (BOTTOM SPECTRUM) from the centerline of the flame, respectively	24
9	TOP SPECTRUM: N <sub>2</sub> CARS spectrum observed 2 mm above the centerline of 0.3 CH <sub>4</sub> -N <sub>2</sub> O flame (•) compared theoretical spectrum calculated at T = 2550 K and C = 62% N <sub>2</sub>  BOTTOM SPECTRUM: N <sub>2</sub> CARS spectrum observed 1 mm above the centerline of a 0.27 CH <sub>4</sub> -N <sub>2</sub> O flame (•) compared to theoretical spectrum calculated at T = 2300 K and C = 33% N <sub>2</sub>	25
10	(I <sub>N<sub>2</sub></sub> /I <sub>N<sub>2</sub>O</sub> ) (•) obtained from CARS spectra taken 1 mm above the burner head of a 0.27 CH <sub>4</sub> -N <sub>2</sub> O flame and corresponding temperatures (•) versus distance from the centerline of the burner	26
11	Experimental (•) and calculated N <sub>2</sub> CARS spectra (solid line) 2 mm above the centerline of the burner surface: BOTTOM, 0.4 flame; TOP, 1.0 flame	27
12	Experimental (•) and calculated N <sub>2</sub> CARS spectra (solid line) from a 0.5 flame at various distances from the burner surface: BOTTOM, 2 mm; TOP, 10 mm	28
13	Experimental (•) and calculated N <sub>2</sub> CARS spectra (solid line) from 0.5 flame at various distances from the burner surface: BOTTOM, 20 mm; TOP, 40 mm	29
14	Temperature versus distance above the burner surface for a 0.5 flame at a flow of 16.8 (•) and 33.4 (o) cm/s	30



## INTRODUCTION

Recently, coherent anti-stokes raman scattering (CARS) spectroscopy has undergone several modifications to enhance its usefulness for investigating flames. CARS can arise from the nonlinear response of homogeneous media. The nonlinear response of a homogeneous medium upon which waves  $\omega_1$  and  $\omega_2$  are incident generates an oscillating polarization. The lowest order nonlinearity is the third order susceptibility,  $\chi^{(3)}(-\omega_3, \omega_1, \omega_1, \omega_2)$ , which generates a frequency component of the polarization at  $\omega_3 = 2\omega_1 - \omega_2$  by the process termed "three wave mixing" (ref 1). Resonant enhancement of three wave mixing occurs if  $\omega_1 - \omega_2$  is made equal to a Raman active vibration,  $\omega_0$ , in which case the enhancement of the signal  $\omega_3$  is termed a CARS process (ref 2). Since CARS is a coherent process,  $\omega_3$  is maximized if the wavevectors,  $k_i$ , are phasematched so that  $2k_1 = k_2 + k_3$  where  $k_i$  equals  $\omega_i n_i / c$ ,  $c$  the speed of light, and  $n_i$  the refractive index at frequency  $\omega_i$ . In gases, which are nearly dispersionless, colinear beams are phasematched. Using this geometry, since CARS is generated by an iterative growth process, the spatial resolution is poor. If  $\omega_1$  is split and phasematching achieved,  $\omega_3$  is maximized and, since CARS generation occurs only where all three beams intersect, the spatial resolution is improved. The split  $\omega_1$  phasematched geometry is termed "BOXCARS" (ref 3). BOXCARS in which the wavevectors are not phasematched in one plane is termed folded (or nonplanar) BOXCARS and has the advantage that  $\omega_3$  is easily spatially isolated from the generating beams (refs 4 through 6).

Conventionally  $\omega_2$  is narrowband and scanned to obtain the spectrum at  $\omega_3$ . However, to obtain spectra in transient and/or turbulent media it is appropriate to use a broadband  $\omega_2$  [ $\sim 150 \text{ cm}^{-1}$  full width at half height (FWHH)] to obtain the full rovibrational spectrum at  $\omega_2$  within the time duration of the laser pulse ( $\sim 10 \text{ ns}$ ) (ref 7). Averaging of the single-shot spectra may be undertaken to improve the signal-to-noise according to the constraints of the experiment.

BOXCARS has been used to obtain temperature and concentration of post-flame gases in stationary flames using broadband (ref 8) and narrow band (ref 9) spectra, and transient flames using single-shot (ref 10) spectra. Recently, laser absorption measurements of the temperature and concentration of radicals have been reported in the thin reaction zone of atmospheric flames (ref 11). CARS measurements in the reaction zone of a flame have not been reported even though BOXCARS has more precisely defined spatial resolution in the direction of the laser beams than line-of-sight methods such as laser absorption. In addition CARS allows direct monitoring of the rovibrational levels of the reactant molecules as they undergo flame decomposition processes.

Because of these capabilities, simultaneous measurement of  $\text{N}_2$  and  $\text{N}_2\text{O}$  CARS was undertaken in the reaction zone of a lean  $\text{CH}_4\text{-N}_2\text{O}$  flame. A lean  $\text{CH}_4\text{-N}_2\text{O}$  flame near lift-off creates sufficiently sharp spatial and temperature gradients to show the capabilities of CARS.  $\text{N}_2\text{O}$  CARS spectra, which have not been previously reported, have structure at lower temperatures than diatomics due to the population of low-lying bending modes.  $\text{N}_2\text{O}$  CARS spectra are especially suitable for studying initial decomposition reaction in a  $\text{CH}_4\text{-N}_2\text{O}$  flame. The measurements were extended for  $\text{N}_2$  CARS to the post flame region of a series of flames with equivalence ratio increasing to 1.0 to evaluate the agreement of temperatures and



concentrations determined from CARS spectra with the results of thermochemical calculations (ref 12).

## EXPERIMENTAL METHOD

CARS spectra were generated using the apparatus shown in figure 1. Non-planar BOXCARS was utilized to achieve phasematching. The output of a Quanta-Ray DCR-1A Nd/YAG laser at 1.06 microns (700 mj) is doubled to generate the pump beam at 5320 Å (250 mj) with a bandwidth near 1 cm<sup>-1</sup>. The pump beam is separated from the primary beam using prisms. The pump beam is split using beam splitter BS1 to generate  $\omega_{1p}$  and  $\omega_{1s}$ .  $\omega_{1s}$  is used to pump a dye laser to generate the Stokes beam,  $\omega_2$ . The dye laser consists of a flowing dye cell in a planar Fabry-Perot oscillator cavity pumped slightly off-axis by 20% of  $\omega_{1s}$  with the output amplified by an additional dye cell pumped by the remainder of  $\omega_{1s}$ . The dye laser was operated broadband using Exciton Rhodamine 640 in dry methanol at a concentration of  $2.4 \times 10^{-4}$  M and  $3.2 \times 10^{-5}$  M in the oscillator and amplifier dye cell, respectively, to produce 30 mj centered at 6060 Å (16502 cm<sup>-1</sup>) with a bandwidth of 121 cm<sup>-1</sup>. To achieve BOXCARS geometry,  $\omega_{1p}$  is again split with beam splitter, BS2, to generate  $\omega_1$  and  $\omega'_1$ . In the optical configuration used to generate non-planar BOXCARS, the  $\omega_1$ ,  $\omega'_1$ , and  $\omega_2$  beams are parallel and situated on a circle of 1 inch diameter at the focusing lens (200 mm focal length) with  $\omega_1$  and  $\omega'_1$  in the central horizontal plane of the lens and  $\omega_2$  below  $\omega_1$  and  $\omega'_1$  in the central vertical plane. Telescopes are inserted in the  $\omega_{1p}$  and  $\omega_2$  beams to allow the focal spot size of both beams to be equalized. The telescopes also allow the position of the  $\omega_1$ ,  $\omega'_1$ , and  $\omega_2$  beamwaists to be adjusted so that they all intersect after focusing. This was achieved using 0.85 and 2x Galilean telescopes in  $\omega_{1p}$  and  $\omega_2$ , respectively. To achieve phasematching a 12.5 mm thick optical flat rotatable about it's horizontal axis was inserted into  $\omega_2$  before focusing. It is adjusted to maximize the  $\omega_3$  signal. The beams were recollimated with a lens (200 mm focal length) after which the  $\omega_3$  was located below the plane of  $\omega_1$  and  $\omega'_1$ .  $\omega_1$ ,  $\omega'_1$ , and  $\omega_2$  were terminated with a neutral density filter (OD4).  $\omega_3$  was focused using a 50 mm focal length lens onto the slits of a 1/4-meter monochromator equipped with a 1,800 line per millimeter grating and 100-micron slits. The signal was detected by a PAR SIT detector and processed by a PAR OMA2 system. Neon lines were used to calibrate the monochromator. The FWHH of the Neon lines nearest  $\omega_3$  were determined to be 6.4 cm<sup>-1</sup> with 2.33 cm<sup>-1</sup> per channel.

Flame measurements were made on a premixed CH<sub>4</sub>-N<sub>2</sub>O flame maintained on a circular burner of 1.4 cm diameter. The burner surface was constructed of a matrix of steel syringe needles of 0.2 cm outer diameter so that a flat flame is obtained under suitable flow conditions. Matheson technical grade methane and chemically pure nitrous oxide were separately flowed through Matheson rotameters prior to premixing. The flow through the burner was adjusted to 16.1 cm/s to maintain a 0.27 fuel-air equivalence ratio flame, which is near lift-off, localized at a few syringe tubes near the center of the burner. The oblong shaped flame increased in size to approximately 5 mm in diameter at 10 mm above the burner surface. Increasing the methane flow to that for a 0.31 equivalence ratio flame gave a flat flame at a flow of 16.3 cm/s. The flow conditions for the other flames used are given in the results section. The center line of the burner was placed at the intersection of the  $\omega_1$ ,  $\omega'_1$ , and  $\omega_2$  beamwaists. The burner was mounted on horizontal and vertical translation stages.

## RESULTS

### Theory

$N_2$  CARS spectra were calculated using the method outlined in reference 13 and  $N_2$  spectral parameters given in references 13 and 14. The observed CARS spectrum is proportional to the square of the modulus of the third order susceptibility,  $\chi^{(3)}$ , which is the sum of a resonant term,  $\chi_r$ , related to a nuclear displacement and a nonresonant term,  $\chi_{nr}$ , related to electronic displacement.

$$\chi^{(3)} = \chi_r + \chi_{nr} \quad (1)$$

The resonant term is calculated as a sum of Lorentian line shapes of each  $Q(J)$  rotational transition

$$\chi_r = \sum_j \frac{k_j \Gamma_j}{2\Delta\omega_j - i\Gamma_j} \quad (2)$$

given that

$$k_j = \frac{2N}{\hbar} / \alpha_j^2 (\Delta p_j^{(o)}) \Gamma_j^{-1} \quad (3)$$

where  $N$  is the number density,  $\alpha_j$  is the isotropic polarizability matrix element

for the transition,  $\Delta p_j^{(o)}$  is the normalized population difference between the molecular energy levels  $j$  involved in the transition,  $\Gamma_j$  is the isolated pressure-broadened linewidth, and  $\Delta\omega_j = \omega_1 - \omega_2 - \omega_j$ . The calculated  $|\chi^{(3)}|^2$  is first convoluted over the laser shapes and then over a triangular instrumental slit function.

$\chi_r$  is the sum of real and imaginary components  $\chi'$  and  $\chi''$ , respectively, so that

$$|\chi^{(3)}|^2 = \chi'^2 + 2\chi' \chi_{nr} + \chi'^2 + \chi_{nr}^2 \quad (4)$$

$\chi'$  and  $\chi''$  display resonant and dispersive behavior with respect to the detuning frequency,  $\Delta\omega_j$ .

As the concentration of the resonant species is lowered the cross term  $\chi' \chi_{nr}$ , which is dispersive, modulates the shape of the spectrum. The observation of dispersively modulated spectra allows estimation of the concentration in addition to the temperature based on model calculations.

As an alternative to determining concentration from the shape of the total spectrum, concentration can be estimated from the ratio of the total CARS intensity,  $I$ , to the nonresonant intensity,  $I_{nr}$ , at any frequency at which a resonant transition of the species occurs. In broadband CARS the nonresonant susceptibility is usually observed directly in regions where no resonance occurs. The spectral distribution of the nonresonant susceptibility which mirrors that of  $\omega_2$ , can be obtained either from measurements of the distribution of  $\omega_2$  or directly from

measurements on a nonresonant gas. The spectral distribution of the nonresonant susceptibility is relatively constant (as can be ascertained by measurements before and after a series of experiments). Therefore, measurement of the nonresonant susceptibility at any frequency in the broadband spectrum will allow estimation of  $I_{nr}$ , the nonresonant susceptibility at the frequency at which the intensity of the resonant transition,  $I$ , occurs. The function  $(I-I_{nr})/I_{nr}$  should be independent of the laser intensity (although of course the precision will be affected by the intensity) and according to equations 2 and 3 vary with concentration quadratically at high concentration and linearly at lower concentration when  $\chi^2 \ll 2\chi'\chi_{nr}$ . If  $I_{nr}$  is estimated at a frequency at which the nonresonant susceptibility begins to have some significant contribution from the resonant susceptibility at higher concentrations a lowering of the quadratic dependence would be observed. This effect would depend on the ratio of the resonant to nonresonant susceptibility cross section for the system under investigation. The effect would be minimized by proper choice of the frequency at which the nonresonant susceptibility is determined.

### Air/Argon Mixtures

$N_2$  CARS spectra were taken at 2 mm above the burner head of mixtures of room temperature premixed air and argon (AIR/AR) flowing through the burner. The composition of the AIR/AR mixtures was set by adjusting the flow of argon and air separately prior to premixing. The total flow for argon was at a rate at which no signal was observed from nitrogen diffusing into the argon flow from the surrounding air. The percentage of air in the mixtures varied from 0% to 30%. The spectra of the mixtures are shown in figures 2 and 3. The compositions of the mixtures for which  $N_2$  CARS spectra were taken are given in table 1. CARS spectra for which the air concentrations were determined from a fit of the total spectra to the calculated spectra are shown in figures 4 and 5. The concentration determined by the best visual match between the calculated and experimental spectra were 9% and 20% air for gas mixtures whose compositions were 8.54% and 19.7%, respectively.

Concentrations determined from the function  $(I-I_{nr})/I_{nr}$  are given in table 1.  $I$  was determined from the intensity of the broadband CARS spectra at the frequency of the maximum of the nitrogen  $Q_{10}$  resonance.  $I_{nr}$ , which was 80% of the peak nonresonant susceptibility at the frequency of  $I$ , was determined from the intensity in the broadband spectra at the frequency at which the nonresonant susceptibility is 80% of the peak value on the other side of the peak of the nonresonant susceptibility curve from that at which the nitrogen resonance occurs to avoid interference from the resonant susceptibility.

The values calculated for  $(I-I_{nr})/I_{nr}$  are shown in figure 6 along with  $(I-I_{nr})/I_{nr}$  determined from model spectra. The calculated and experimental  $\log(I-I_{nr})/I_{nr}$  agreed closely as can be seen from figure 6. The percent of air in the mixtures (table 1) was determined from the theoretical curve given in figure 6. For higher concentration the slope of the curve is near two. The slope as expected decreases for lower concentration. The agreement between the experimentally determined and known percent of air was 6.1%. In this method of determining composition it is not necessary to obtain a calibration curve since the experimental and theoretical spectra are in good agreement. In addition, this



method offers rapid data reduction of large amounts of data with reasonable accuracy. Fitting the full spectrum by a least squares method should give increased precision.

### Reaction Zone Spectra

Broadband  $N_2$  and  $N_2O$  spectra were obtained from the reaction zone of both the 0.27 and 0.30 equivalence ratio flames. In addition,  $N_2$  spectra were obtained in the post-flame region of these flames. The 0.27 equivalence ratio flame was scanned horizontally from the outer wall of the burner to the centerline at a height of 1 mm above the burner surface.  $N_2$  and  $N_2O$  spectra obtained from the region of largest concentration and temperature gradient prior to the disappearance of  $N_2O$  are shown in figure 7. The 0.30 equivalence ratio flame, which was a flat flame, was scanned vertically along the center line. Spectra similar to that shown in figure 7 were obtained below the region of maximum temperature.

To identify  $N_2O$  CARS spectra, which had not been reported previously, CARS spectra were also taken 1 mm above the centerline of the burner with room temperature  $N_2O$  gas flowing through the burner at a velocity sufficient to remove  $N_2$  from the sampling volume. Spectra were taken above both a room temperature burner and a burner heated by heat transfer from a flame extinguished immediately prior to the measurement. The room temperature  $N_2O$  spectra had a prominent peak at  $2224.7\text{ cm}^{-1}$  with a low intensity shoulder at  $2208.8\text{ cm}^{-1}$ . The spectra taken above the hot burner showed four peaks of progressively diminishing intensity at  $2224.7$ ,  $2208.8$ ,  $2192.8$ , and  $2174.7\text{ cm}^{-1}$ . Similar peaks have been observed at  $2223.8$ ,  $2209.5$ , and  $2195.6\text{ cm}^{-1}$  in the infrared and Raman at 337 K and assigned to  $\nu_3$ ,  $\nu_3 + \nu_2 - \nu_2$  and  $\nu_3 + 2\nu_2 - 2\nu_2$  where  $\nu_1$ ,  $\nu_2$ , and  $\nu_3$  are the NO stretch at 1285, the bend at 558.8 and the NN stretch at  $2223.5\text{ cm}^{-1}$ , respectively (ref 15). The positions of  $\nu_3$ ,  $\nu_3 + \nu_2 - \nu_2$ ,  $\nu_3 + 2\nu_2$  and  $\nu_3 + 3_2 - 3_2$ , using Susuki's values (ref 16) for the spectroscopic constants are calculated to occur at  $2223.5$ ,  $2201.5$ ,  $2195.3$ , and  $2180.3\text{ cm}^{-1}$  in good agreement with the  $N_2O$  peak position observed in the spectrum taken above the hot burner. The spectra taken in the flame (fig. 7) show, in addition to a peak attributable to the  $N_2$  Q branch fundamental,  $Q_{10}$ , at  $2330\text{ cm}^{-1}$  and associated hot bands, the same peaks that occur in  $N_2O$  above the hot burner. An expanded version of the spectrum taken 1.4 mm from the centerline is shown in figure 8. This spectrum clearly shows the resolved structure of hot  $N_2O$ .

The spectra shown in figure 7 and similar spectra taken at other positions in the flame allow the determination of temperature and concentration of  $N_2$  and  $N_2O$ . Comparison of the half width of the nitrogen  $Q_{10}$  transition and the modulation of spectra by the nonresonant susceptibility with model calculations allows the estimation of temperature to  $\pm 100\text{ K}$  and concentration to  $\pm 10\%$  when no hot bands are observed. Observation of hot bands allows least squares fitting of the calculated and experimental Q peak maxima to give temperature to  $\pm 50\text{ K}$  and concentration to  $\pm 5\%$  based on replicate determinations. Calculated spectra are shown in figures 8 and 9. The temperature and concentrations estimated for the 0.27 flame are given in table 2.

In addition, the concentration of  $N_2O$  can be estimated from the resonant and nonresonant intensity at  $\nu_3$  as discussed. Knowing the spectrum of the nonresonant susceptibility, the nonresonant intensity at  $\nu_3$  can be obtained from each broadband spectrum. The square root of the ratio of the resonant to nonresonant intensity, which is linear with concentration, was used to obtain  $N_2O$  concentration utilizing the broadband  $N_2O$  spectrum at room temperature for calibration. In this case experimental calibration is needed since the  $N_2O$  CARS spectra were not calculated. (The effect of temperature, which was small since both the resonant and nonresonant susceptibility scale similarly with temperature, was determined from model calculations). Having obtained the concentration of  $N_2O$ , the  $N_2$  concentration can be obtained from the ratios of  $N_2$  to  $N_2O$  intensity (fig. 10) taking into account that resonant cross section of  $N_2O$  is 0.53 that of  $N_2$  (ref 17).

### Post-Flame Spectra

The agreement of temperature and concentration obtained from  $N_2$  CARS spectra with the results of thermochemical calculations (table 3) was investigated in the post-flame gases of lean and stoichiometric flames. Temperature and concentration were determined along the centerline of the burner as a function of distance above the burner. The temperature as indicated by the height of the  $Q_{21}$  and  $Q_{32}$  nitrogen hot bands increased with the rate of flow. As discussed, in a 0.3 flame at 2 mm above the burner  $N_2O$  was observed along with  $N_2$ . At 3 mm and 4 mm above the burner surface,  $N_2$  was observed at temperatures of 2350 K and 2453 K, respectively. At 5 mm the temperature and concentration (table 2) were determined from the spectra shown in figure 9. Above 5 mm (up to 6 cm) the temperature decreased while the concentration remained constant within experimental error. In lean and stoichiometric flames investigated with equivalence ratios higher than 0.3, at sufficiently high flow rates,  $N_2O$  was not observed and  $Q_{21}$  and  $Q_{32}$   $N_2$  relative heights indicated temperatures substantially above the values given by the thermochemical calculations with  $Q_{32}$  indicating temperatures higher than  $Q_{21}$  and up to 4000 K in some instances. The cause of these anomalous spectra is presently being investigated. At lower flow rates the spectra (fig. 11) obtained 2 mm above the burner surface in 0.4, 0.5 and 1.0 flames in addition to the 0.3 at 5 mm, gave temperatures and concentrations (table 4) consistent with the thermochemical calculations.

The experimental precision of the temperatures and concentrations was determined by comparison of four replicate measurements on the 1.0 flame. The error determined in this manner is consistent with the photon statistics of the measurements. The percent error in the measurements for the other flames should be similar since all the spectra were summed (200 scans) to give near to 10,000 counts at  $Q_{10}$ .

At a lower flow rate in the 0.5 flame lower temperatures were obtained. The profiles in the 0.5 flame at flows of 16.9 and 33.4 cm/s are given in tables 5 and 6, respectively. The  $N_2$  spectra at the higher flow are shown in figures 12 and 13. A comparison of the differing profiles is given in figure 14. In the 1.0 flame, lower flame velocity resulted in flashback before any lowering in measured temperature was observed.

To summarize, in the 0.3 flame close to the burner surface (1 mm above)  $N_2O$  spectra along with  $N_2$  spectra were observed. Higher above the burner surface (5 mm) a maximum temperature and concentration in agreement with thermochemical calculations was observed. In the 0.4 flame at the same flow, 16.8 cm/s and position in the flame  $N_2O$  was not observed and the measured temperature and concentration are in close agreement with theory. In the 0.5 flame at nearly the same flow temperatures lower than theory are measured. At sufficiently high flow, 56.7 and 60.5 cm/s in the 0.5 and 1.0 flames, respectively, anomalous spectra giving apparent temperature much higher than theory were encountered. In the 0.5 and 1.0 flames, at flow intermediate between striking back and those at which anomalous spectra were encountered, the temperature and concentration were consistent within experimental error with theory. The intermediate range of flows at which agreement with theory was obtained increased with the calculated flame temperature as the equivalence ratio was increased toward 1.0.

## DISCUSSION

Measurements were made in AIR/AR mixtures to assess the use of CARS to determine concentration. Visually matching the shape of modulated CARS spectra with the results of model calculations for 9% and 20% AIR mixtures gives results within the accuracy of the flow meters (5%). A least squares fit of all the points would improve the precision. Alternately, comparing the experimental function  $(I - I_{nr})/I_{nr}$  obtained from two experimental points with the theoretical function  $(I - I_{nr})/I_{nr}$  versus concentration also allows evaluation of the concentration to close to the accuracy of the flow meters. These methods of obtaining concentration were used in obtaining the reaction zone and post-flame region results.

CARS  $N_2O$  spectra obtained above both room temperature and heated burner heads are in good agreement with previously reported Raman and infrared spectra (ref 15) and with the results of calculations made using the spectral constants of Suzuki (ref 16). CARS  $N_2O$  spectra has the advantage of having structure useful for making measurements of temperature and concentration at much lower temperatures than diatomics such as nitrogen. From the temperature obtained from  $N_2$  spectra (table 2) the normalized intensity of the  $N_2O$   $\nu_3 + \nu_2 - \nu_2$  band relative to  $\nu_3$  is greater than 0.1 above 600 K, whereas the normalized intensity of the  $N_2$   $Q_{21}$  band does not reach 0.1 until the temperature exceeds 1500 K. The higher intensity of the  $N_2O$   $\nu_3 + \nu_2 - \nu_2$  band arises from the low energy and double degeneracy of the  $\nu_2$  vibration. Thus  $N_2O$  and similar triatomics are especially valuable for characterizing the lower temperature regions of the profiles obtained in the 0.27 flame. In this region the  $N_2$  spectra were not sufficiently intense to precisely estimate temperature. The complete modeling of  $N_2O$  CARS spectra which is now underway will allow these calculations to be made.

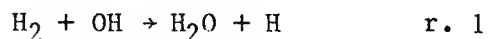
The simultaneous observation of  $N_2$  spectra along with  $N_2O$  spectra allows determination of  $N_2$  to  $N_2O$  relative concentration,  $N_2$  and  $N_2O$  temperature and concentration. The random error in the  $N_2O$  resonant to nonresonant intensity ratios depend solely on the photon statistics of the measurements. (In the worst case the resultant error would be 5% in  $N_2$  concentration). The accuracy of the  $N_2$  concentrations determined from the relative intensity of  $N_2$  to  $N_2O$  also depends on the relative ratios of the Raman cross sections. The  $N_2$  temperature and



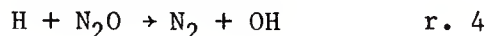
concentrations determined from the shape of the  $N_2$  CARS signal depends on the  $N_2$  spectral parameters and the spectral simulation model which together have been estimated to give errors of  $\pm 100$  K at low temperature and 10% in concentration in flames when only  $N_2$   $O_{10}$  is observed. The average difference between  $N_2$  concentration determined from intensity ratio and band shape is only 10% which is consistent with the estimated error in the methods used. When additional hot bands are observed the precision is increased to  $\pm 50$  K in temperature and 5% in concentration.

The data in figure 10 give insight into the chemical and physical processes occurring in the very spatially inhomogeneous 0.27 flame.  $N_2$  from the surrounding air diffuses into the flame for a distance of approximately 2 mm at which point  $N_2$  CARS spectra is no longer observed (fig. 10).  $N_2$  is again observed when measurements are made closer than 2.3 mm from the centerline of the flame. The  $(N_2/N_2O)^{1/2}$  ratio then rises exponentially as measurements closer to the flame are made with a concomitant rise in temperature.

$H_2$ - $N_2O$  flames have been studied in detail using mass spectrometric means to obtain concentration (ref 18). From these studies it is suggested that the  $H_2$ - $N_2O$  flame has a two-stage reaction zone. In the first stage ( $T < 1700$  K) the kinetics follow the usual bimolecular elementary steps of the hydrogen-oxygen system:

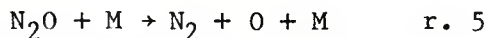


plus reaction

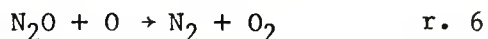


where  $k_4 = 6 \times 10^{13} \exp(-13100/RT) \text{ cm}^3 \text{ mole}^{-1} \text{ s}^{-1}$  all these reactions are characterized by a relatively low activation energy.

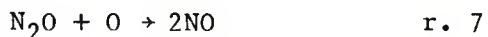
The second stage ( $T > 1700$  K) is dominated by the unimolecular decomposition of  $N_2O$



where  $k_5 = 1.3 \times 10^{15} \exp(-56500/RT)$ . Molecular oxygen is produced via



and NO via



where  $k_6 = 5.4 \times 10^{14} \exp(-32000/RT) \text{ cm}^3 \text{ mole}^{-1} \text{ s}^{-1}$  with  $k_6/k_7 = 3.2$ .



The data given in table 2 and figure 10 are consistent with the kinetics proposed above for stage one, in that  $N_2$  is observed to occur at temperatures below the 1700 K at which the stage two reactions become significant. Thus reaction 4 is seen as a possible source of the  $N_2$  observed at low temperature in the  $CH_4-N_2O$  flame. Further kinetic analysis particularly dependent on temperature and concentration from  $N_2O$  spectra, will determine whether reaction 4 can quantitatively account for the  $N_2$  and  $N_2O$  profiles observed in the  $CH_4-N_2O$  flame.

In the post-flame region the variation of measured temperature with flow can be partially accounted for by the variation of the position of the reaction zone with respect to the burner as a function of flow. In the 0.3 flame, the burning velocity is sufficiently low to be displaced by a flow of 16.8 cm/s above the burner surface to allow observation of  $N_2O$  spectra from the reaction zone. As the burning velocity increases for the flames with increased equivalence ratio the flow is not sufficient to allow observation of  $N_2O$ ; however, temperature is observed to increase with flow which indicates that the reaction zone is displaced sufficiently above the burner surface to inhibit heat lost to the burner. The displacement of the reaction zone above the burner surface so that heat loss to the surface is inhibited is consistent with the agreement within experimental error of the measured and calculated flame temperatures (refs 19 and 20). The anomalously high temperature indicated at still higher flows is perhaps related to distortion of the reaction zone by turbulence induced by the high flow (refs 19 and 20). Further work is needed to interpret the spectra at high flow.

Broadband CARS has been shown to provide temperature and concentration with good precision for major flame species which can perhaps be extended to transients with resonance enhancement. The spatial resolution of the technique was adjusted to obtain information from the thin resolution zone ( $<1$  mm) of the atmospheric  $CH_4-N_2O$  flame. The technique also has the potential for time resolved single shot (10 ns) measurements for use in transient media. These capabilities as has been shown in the  $CH_4-N_2O$  flame can be used to obtain information on the elementary reactions occurring in both transient and stationary flames.



## REFERENCES

1. N. Bloembergen, Nonlinear Optics, Benjamin, New York, 1965.
2. B. I. Greene, R. B. Weisman and R. M. Hochstrasser, Chem Phys, Letters 59, 1978, p 5.
3. A. C. Eckbreth, Appl Phys, Letters 32, 1978, p 421.
4. R. L. Farrow, P. L. Mattern and L. A. Rahn, Sandia Laboratories Report 80-8640, 1980.
5. J. A. Shirley, R. J. Hall and A. C. Eckbreth, Opt Letters 5, 1980, p 380.
6. Y. Prior, Appl. Opt. 19, 1980, p 1741.
7. W. B. Roh, P. W. Schreiber and J. P. E. Taran, Appl. Phys., Letters 29, 1976, p 174.
8. A. C. Eckbreth and R. J. Hall, Combustion Science and Technology, vol 25, 1981, p 175.
9. K. Muller - Dethlefs, M. Pealat and J. P. E. Taran, Ber. Bunsenges Phys. Chem., vol 85, 1981, p 803.
10. L. E. Harris and M. E. McIlwain, Combustion and Flame, vol 48, 1982, p 97.
11. M. S. Chou, A. M. Dean and D. Stern, J. Chem Phys, vol 76, 1982, p 5334.
12. S. Gordon and B. J. McBride, "Computer Program for Calculation of Complex Chemical Equilibrium Compositions, Rocket Performance, Incident and Reflected Shocks, and Chapman-Jouquet Detonations," NASA SP-273, 1976.
13. R. J. Hall, Combustion Flame, vol 35, 1979, p 47.
14. A. Owyong and L. A. Rahn, J. Quant. Elect., vol QE15, 1979, p 25D.
15. C. Dreyfus, L. Berreby and T. Nguyen - Tan, J. Chem Phys, vol 76, 1982, p 755.
16. I. Suzuki, J. Mol. Spectry., vol 32, 1969, p 54.
17. D. G. Fouche and R. K. Chang, Appl. Phys., Letters 20, 1972, p 256.
18. V. P. Balakhnine, J. Vandooren and P. J. Van Tiggelen, Combustion Flame, vol 28, 1977, p 165.
19. A. G. Gaydon and H. G. Wolfhard, Flames, John Wiley, New York, 1969, pp 92-146.
20. I. Glassman, Combustion, Academic Press, New York, 1977, pp 87-105.



Table 1. Concentration of air (%) in air/ar mixtures at 300 K

Concentration		Difference between columns 1 and 2	% Difference between columns 1 and 2
Experimental (%)	Calculated (%)		
7.06	5.92	1.1	16.1
8.54	7.80	0.7	8.7
12.0	11.6	0.4	3.3
13.8	14.8	-1.0	7.2
19.7	18.8	0.9	4.5
22.8	22.7	0.1	0.50
30.2	31.0	<u>-0.8</u>	<u>2.65</u>
Mean ( $\sigma$ )		0.7 (0.3)	6.1 (5.1)

Table 2. Temperature and concentration in the reaction zone of a  $\text{CH}_4\text{-N}_2\text{O}$  flame (2 mm above the burner)

Distance from flame center (mm)	Concentration from intensity (%)		Concentration and temperature from $\text{N}_2$ spectral shape	
	$\text{N}_2\text{O}$	$\text{N}_2$	$\text{N}_2$ (%)	T(K)
0			33	2300
1.14	0	--	20	1200
1.27	20	19	17	900
1.40	28	15	14	800
1.52	43	11	10	600
1.65	58	9.4		
1.78	69	7.9		
2.03	83	6.0		
2.16	93	--		

Table 3. Thermochemical calculations for CH<sub>4</sub>-N<sub>2</sub>O flames

$\phi$ Species	<u>0.1</u>	<u>0.3</u>	<u>0.4</u> Composition	<u>0.5</u> (%)	<u>0.7</u>	<u>1.0</u>
CO	0.02	0.43	0.99	1.77	3.80	7.35
CO <sub>2</sub>	1.62	4.28	5.14	5.69	6.09	5.66
H	—	0.11	0.27	0.50	1.14	2.30
H <sub>2</sub>	—	0.14	0.32	0.59	1.43	3.55
H <sub>2</sub> O	3.13	8.46	10.66	12.60	15.90	19.30
N <sub>2</sub>	64.82	61.64	60.03	58.40	55.40	51.28
NO	1.33	2.25	2.42	2.43	2.17	1.48
O	0.12	0.79	1.21	1.54	1.87	1.58
OH	0.27	2.53	2.27	2.93	3.81	4.02
O <sub>2</sub>	28.69	20.37	16.71	13.50	8.41	3.49
T(K)	21.72	25.41	26.54	27.38	28.46	29.20

Table 4. Measured and calculated temperature (K) and N<sub>2</sub> concentration (%) in a CH<sub>4</sub>-N<sub>2</sub>O flame

HT(mm)	5	2	2	2
Flow (cm/s)	16.8	16.8	33.4	51.7
	<u>Equivalence ratio (F/O)</u>			
	<u>0.3</u>	<u>0.4</u>	<u>0.5</u>	<u>1.0</u>
TEXP	2550	2688	2782	2982 ± 52 (2%)
TCALC	2541	2654	2738	2920
CEXP	60	58	54	45 ± 3 (6%)
CCALC	62	60	58	51

Table 5. Temperature and  $N_2$  concentration profile in a  $CH_4-N_2O$  flame  
( $\phi = 0.5$ ) at a flow of 16.9 cm/s (TCALC = 2734K, CCALC = 58%)

<u>Height above burner (mm)</u>	<u>Temperature (K)</u>	<u>Concentration (%)</u>
3	2566	54.7
5	2559	46.5
10	2563	46.5
15	2491	51.6
20	2320	47.6
30	2090	51.9
40	1840	49.6
50	1820	50.5
60	1700	51.8

Table 6. Temperature and  $N_2$  concentration profile in a  $CH_4-N_2O$  flame  
( $\phi = 0.5$ ) at a flow of 33.4 cm/s (TCALC = 2734K, CCALC = 58%)

<u>Height above burner (mm)</u>	<u>Temperature (K)</u>	<u>Concentration (%)</u>
3	2782	54.2
10	2742	55.3
20	2713	50.8
30	2631	47.2
40	2521	51.1
50	2404	50.7
60	2282	51.4





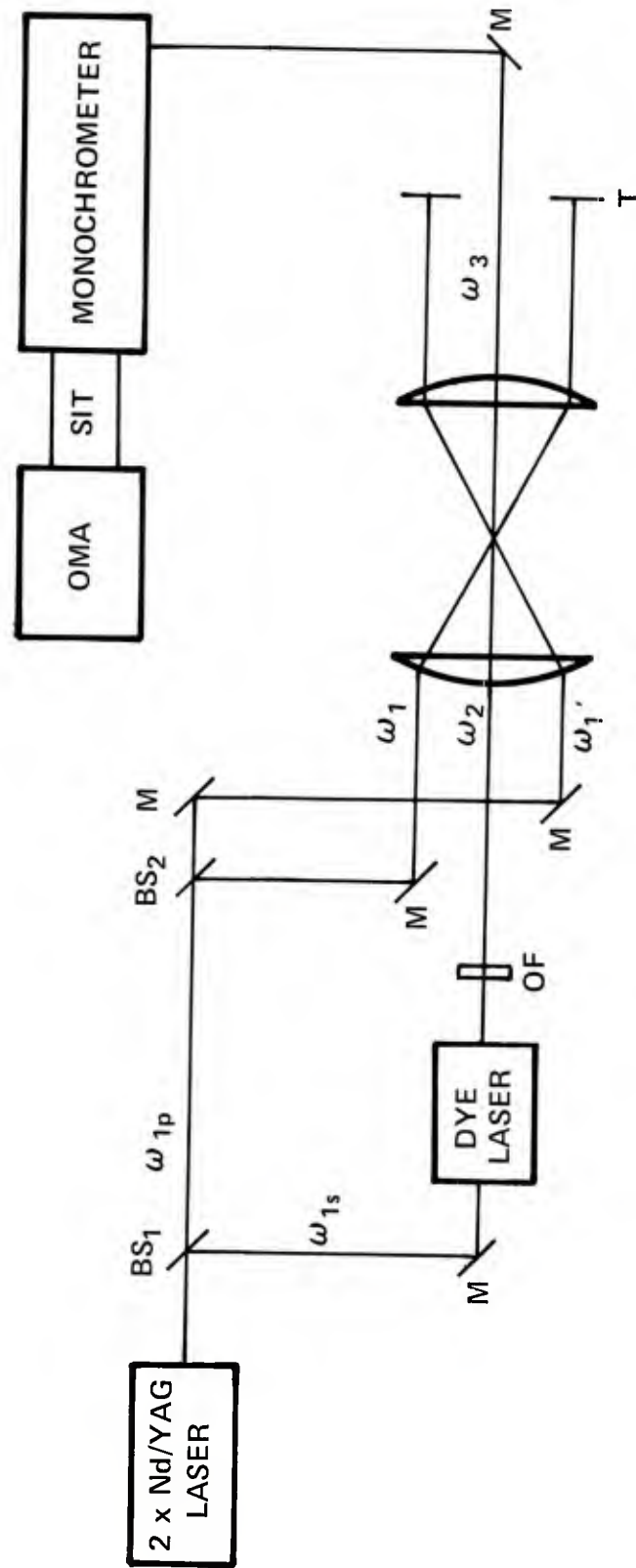


Figure 1. Nonplanar BOXCARS spectrometer where BS is a 50% beam splitter, M is a Mirror, OF is an optical flat rotatable about its horizontal axis and T is a beam terminator

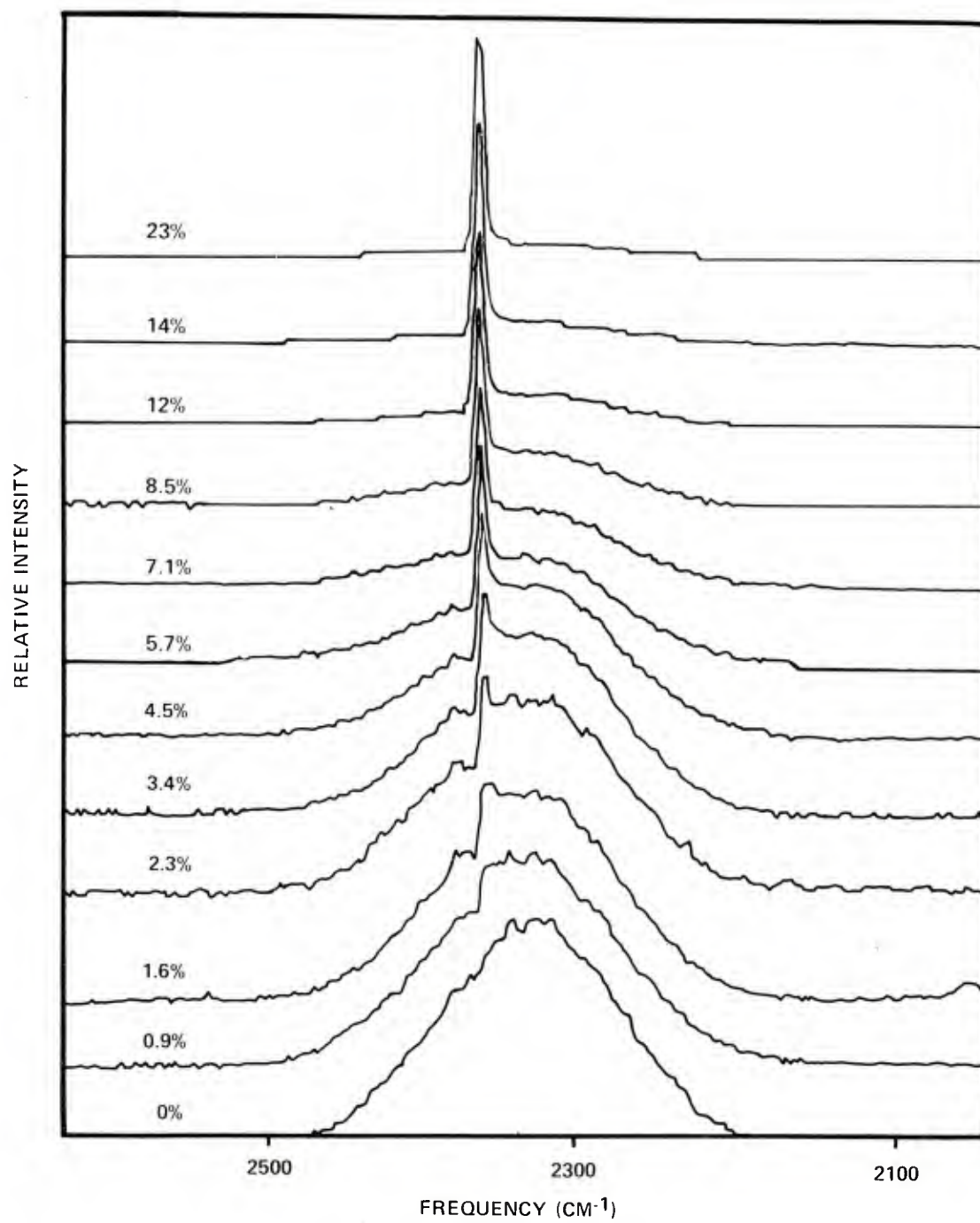


Figure 2. Normalized nitrogen CARS spectra from room temperature air/argon mixtures containing 0% to 23% air

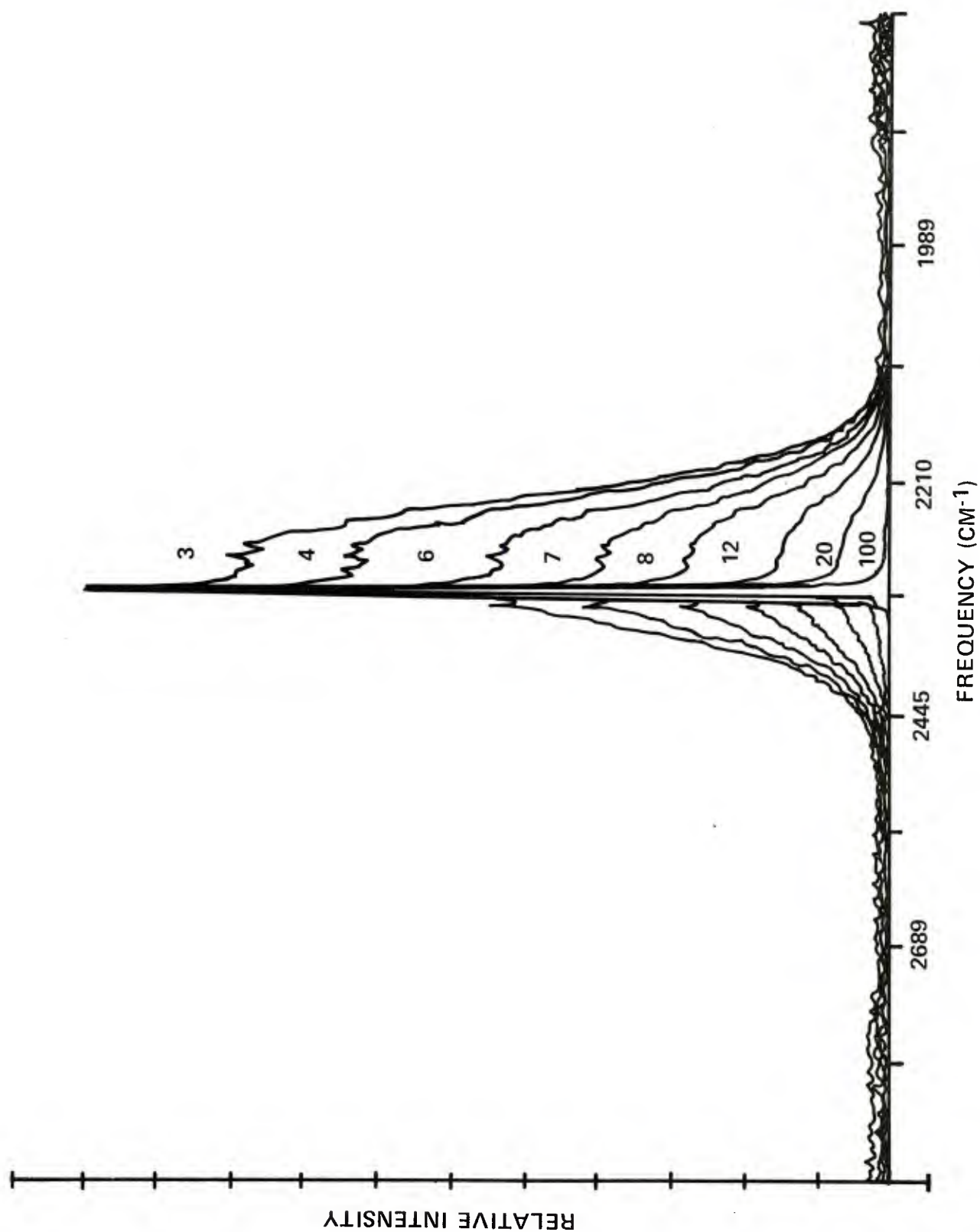


Figure 3. Normalized nitrogen CARS spectra from room temperature air/argon mixtures containing 3% to 100% air

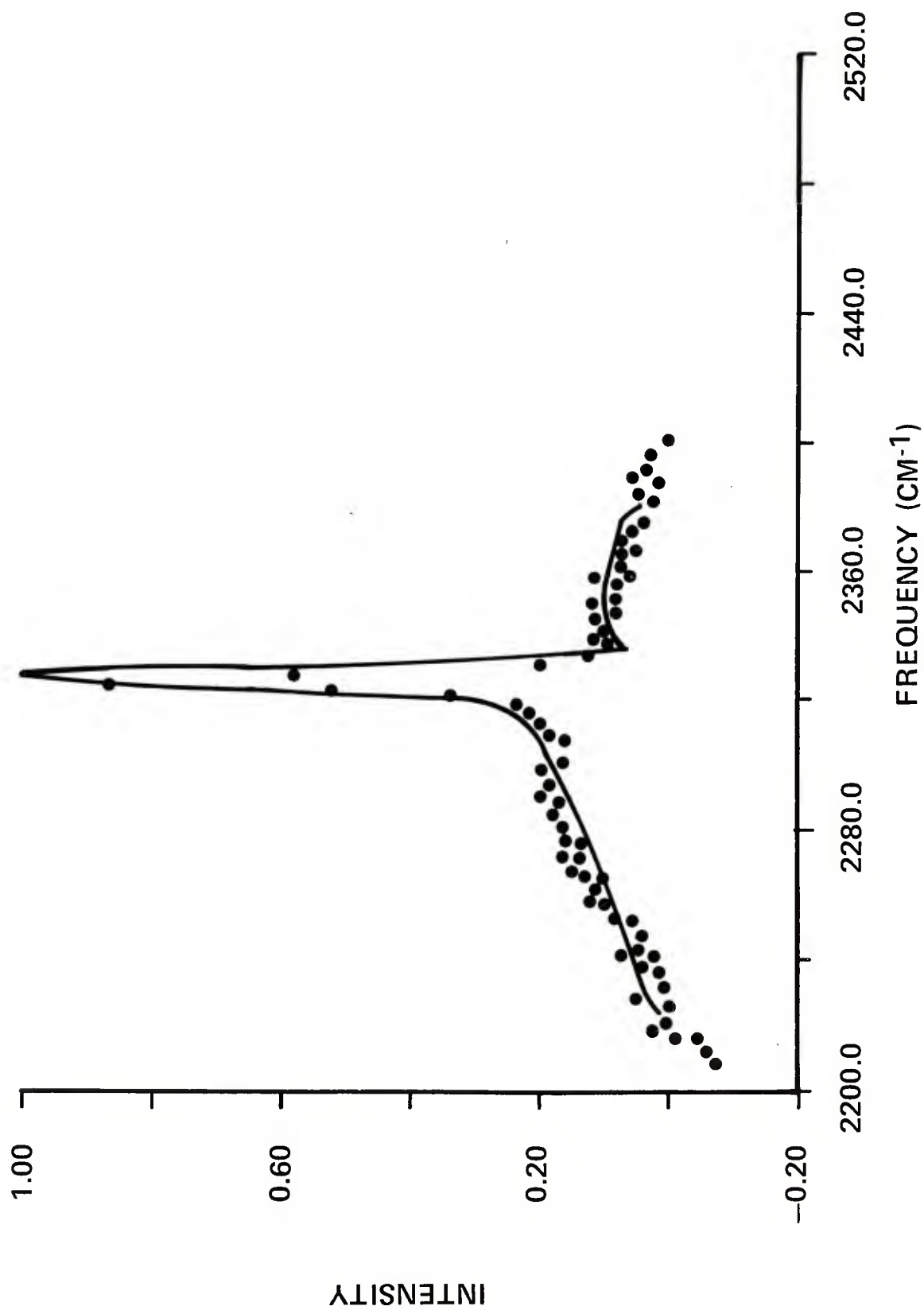


Figure 4. Experimental (·) and calculated N<sub>2</sub> CARS spectra at room temperature in a 9% air/argon mixture (nonplanar CARS)

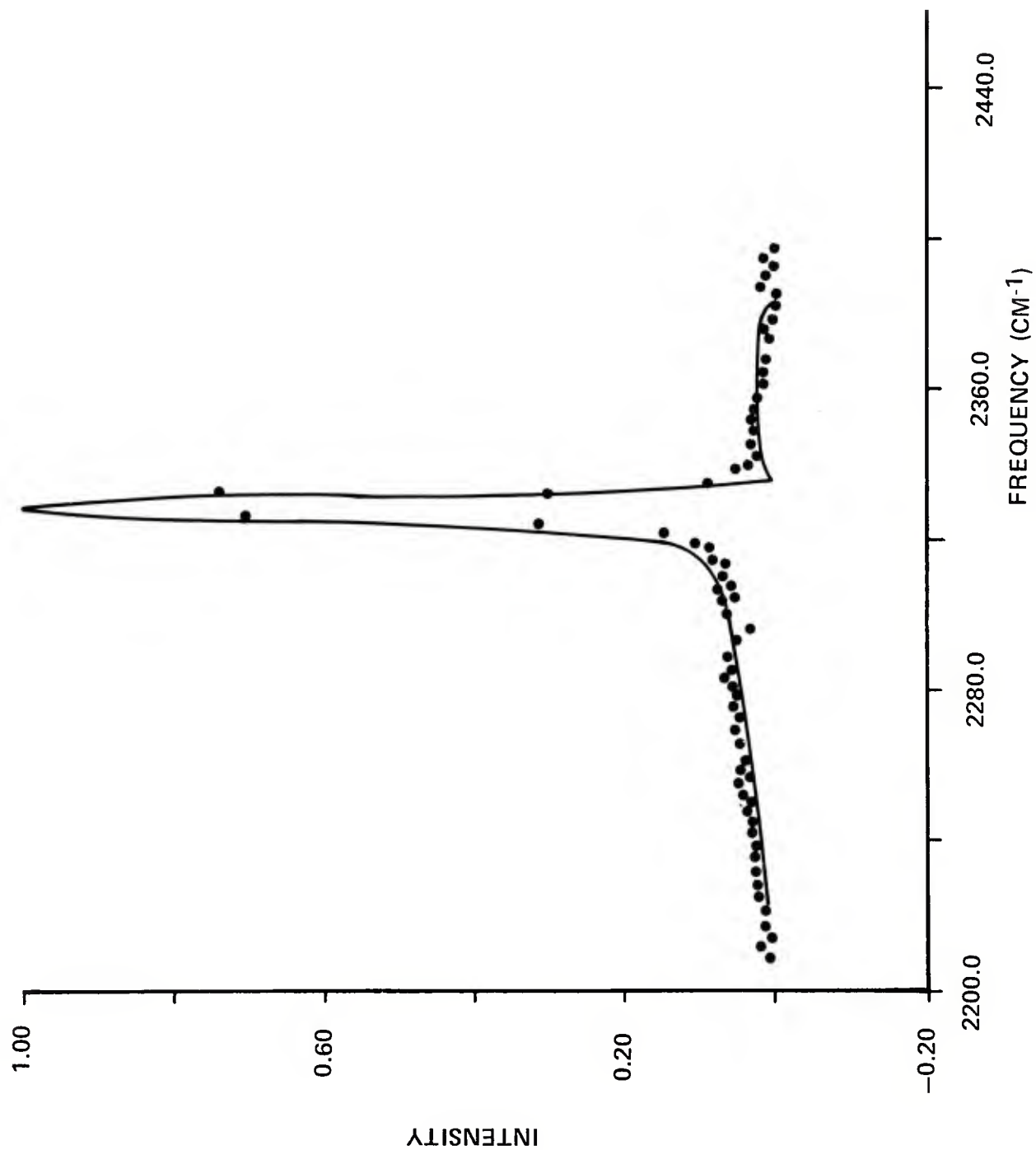


Figure 5. Experimental (•) and calculated N<sub>2</sub> CARS spectra at room temperature in a 20% air/argon mixture (nonplanar CARS)

## AIR/AR MIXTURES AT 300K

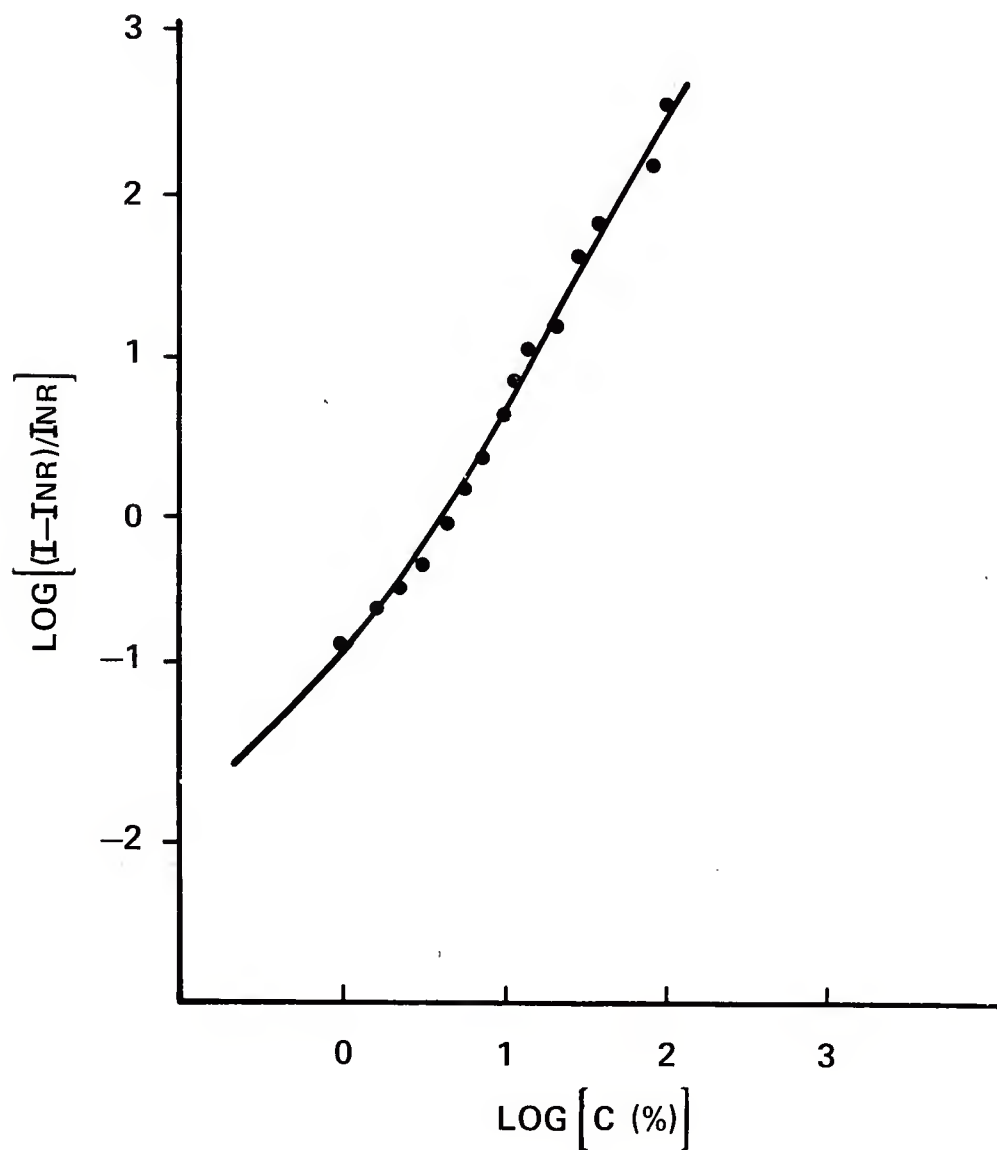


Figure 6. Experimental (•) and theoretical  $\log (I_{10} - I_{nr})/I_{nr}$  where  $I_{10}$  and  $I_{nr}$  are the maximum intensities of nitrogen  $Q_{10}$  and the nonresonant susceptibility versus  $\log [C(\%)]$



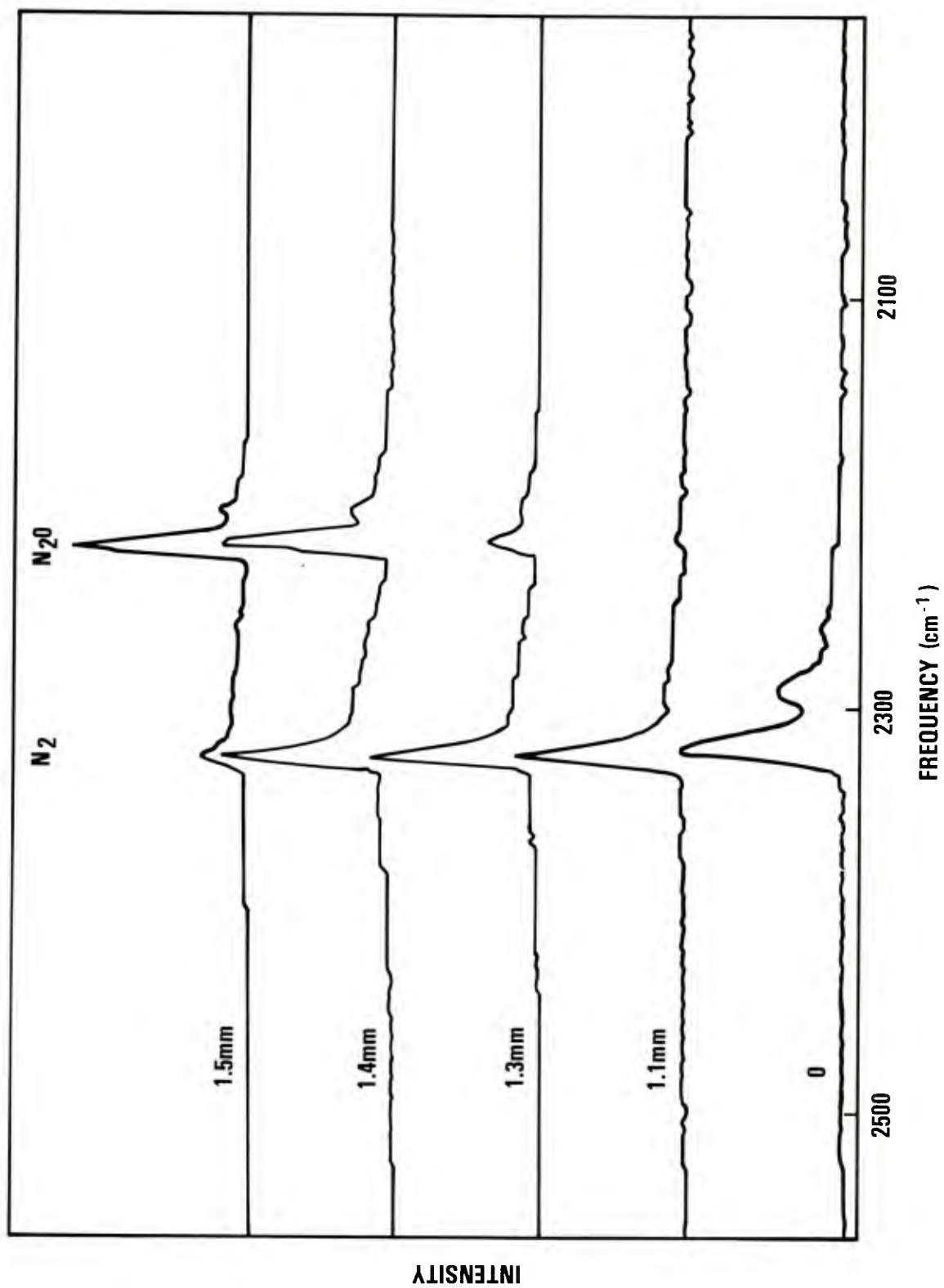


Figure 7. CARS spectra observed 1 mm above the burner head in a 0.27  $\text{CH}_4\text{-N}_2\text{O}$  flame (the distance indicated is from centerline of the burner)

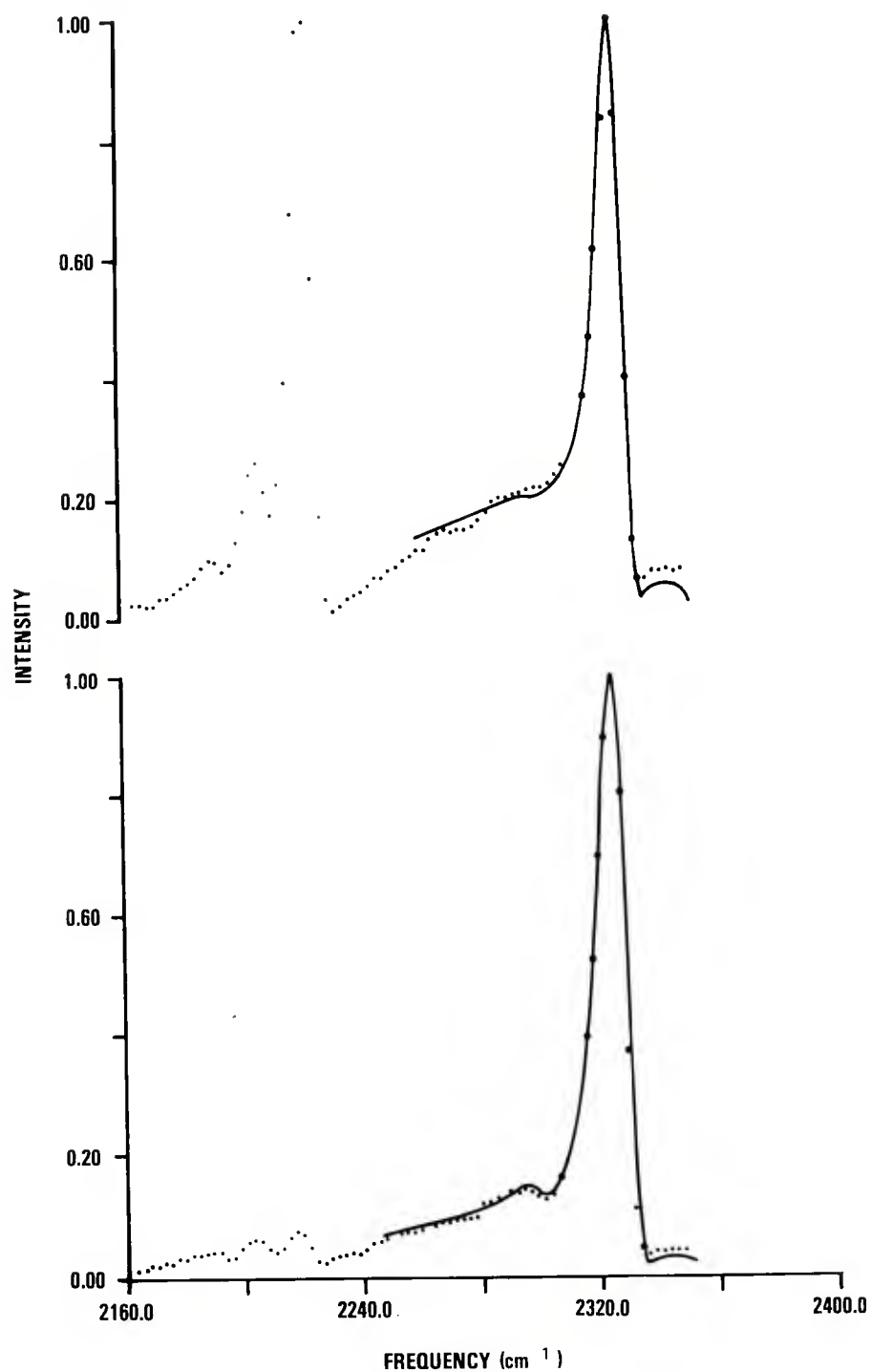


Figure 8. CARS spectra observed 1 mm above the burner head in a 0.27 CH<sub>4</sub>-N<sub>2</sub>O flame (•) compared to theoretical spectra (solid line), calculated at T = 800 K and C = 14% N<sub>2</sub> and T = 1200 and C = 20% N<sub>2</sub> for spectra obtained 1.40 (TOP SPECTRUM) and 1.14 mm (BOTTOM SPECTRUM) from the centerline of the flame, respectively

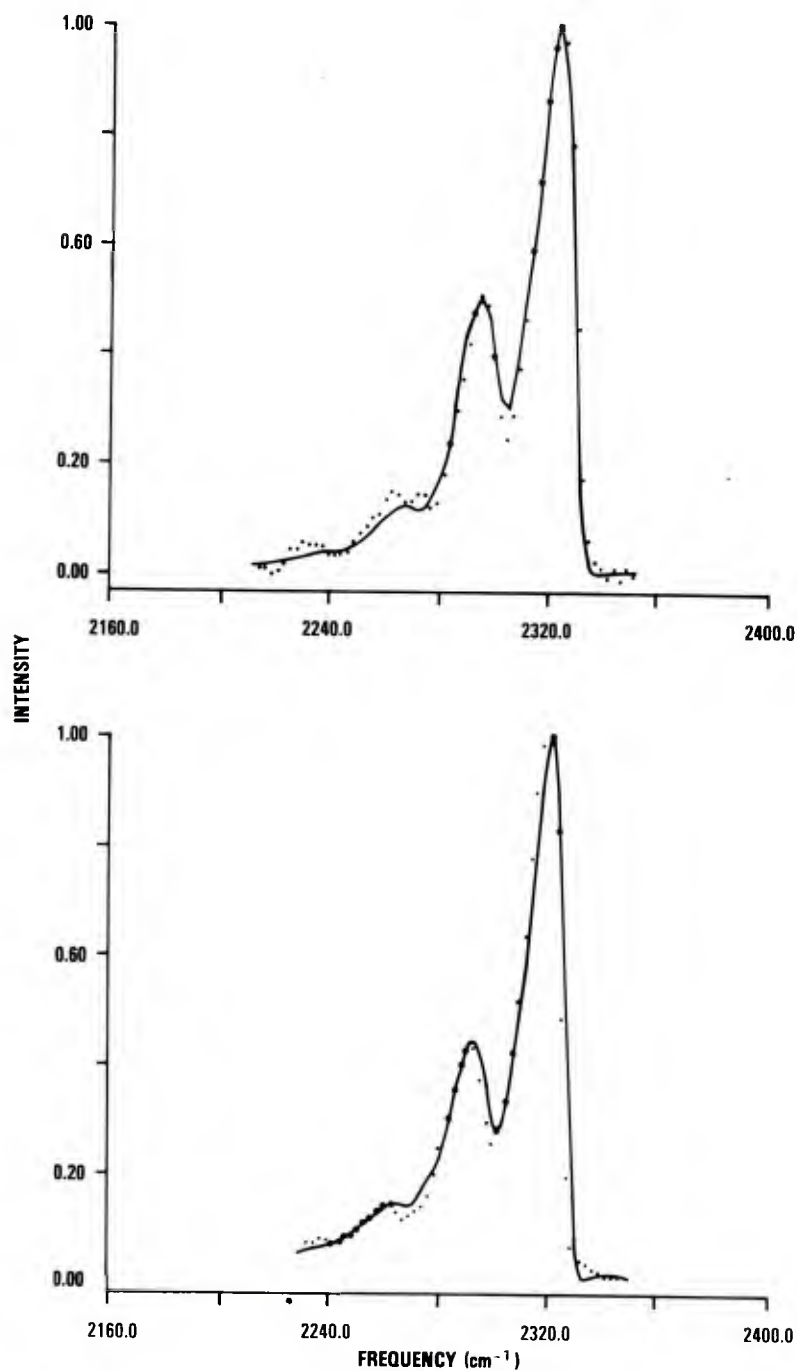


Figure 9. TOP SPECTRUM: N<sub>2</sub> CARS spectrum observed 2 mm above the centerline of 0.3 CH<sub>4</sub>-N<sub>2</sub>O flame (•) compared theoretical spectrum calculated at T = 2550 K and C = 62% N<sub>2</sub>

BOTTOM SPECTRUM: N<sub>2</sub> CARS spectrum observed 1 mm above the centerline of a 0.27 CH<sub>4</sub>-N flame (•) compared to theoretical spectrum calculated at T = 2300 K and C = 33% N<sub>2</sub>

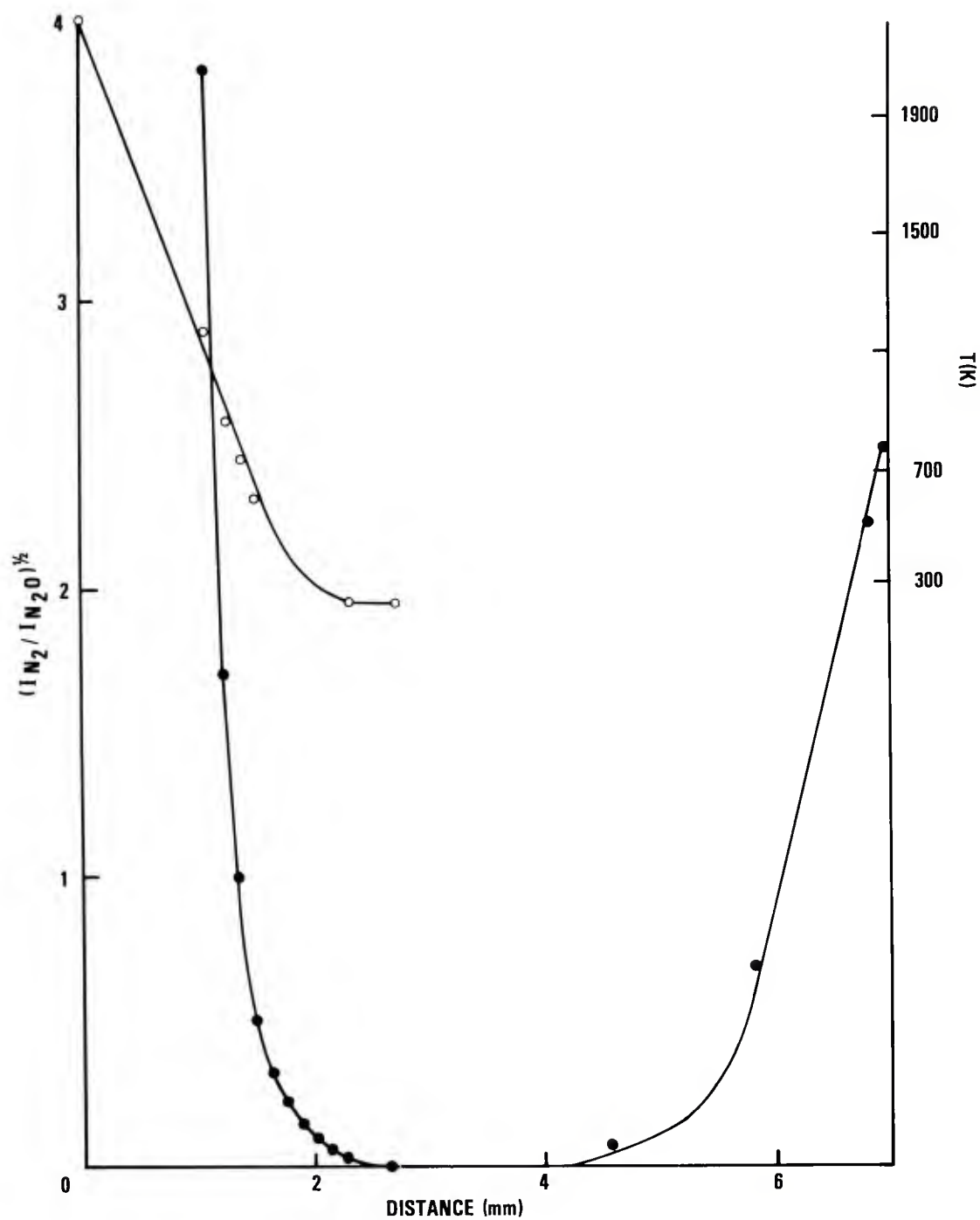


Figure 10.  $(I_{N_2}/I_{N_2O})$  (•) obtained from CARS spectra taken 1 mm above the burner head of a 0.27  $CH_4$ - $N_2O$  flame and corresponding temperatures (•) versus distance from the centerline of the burner

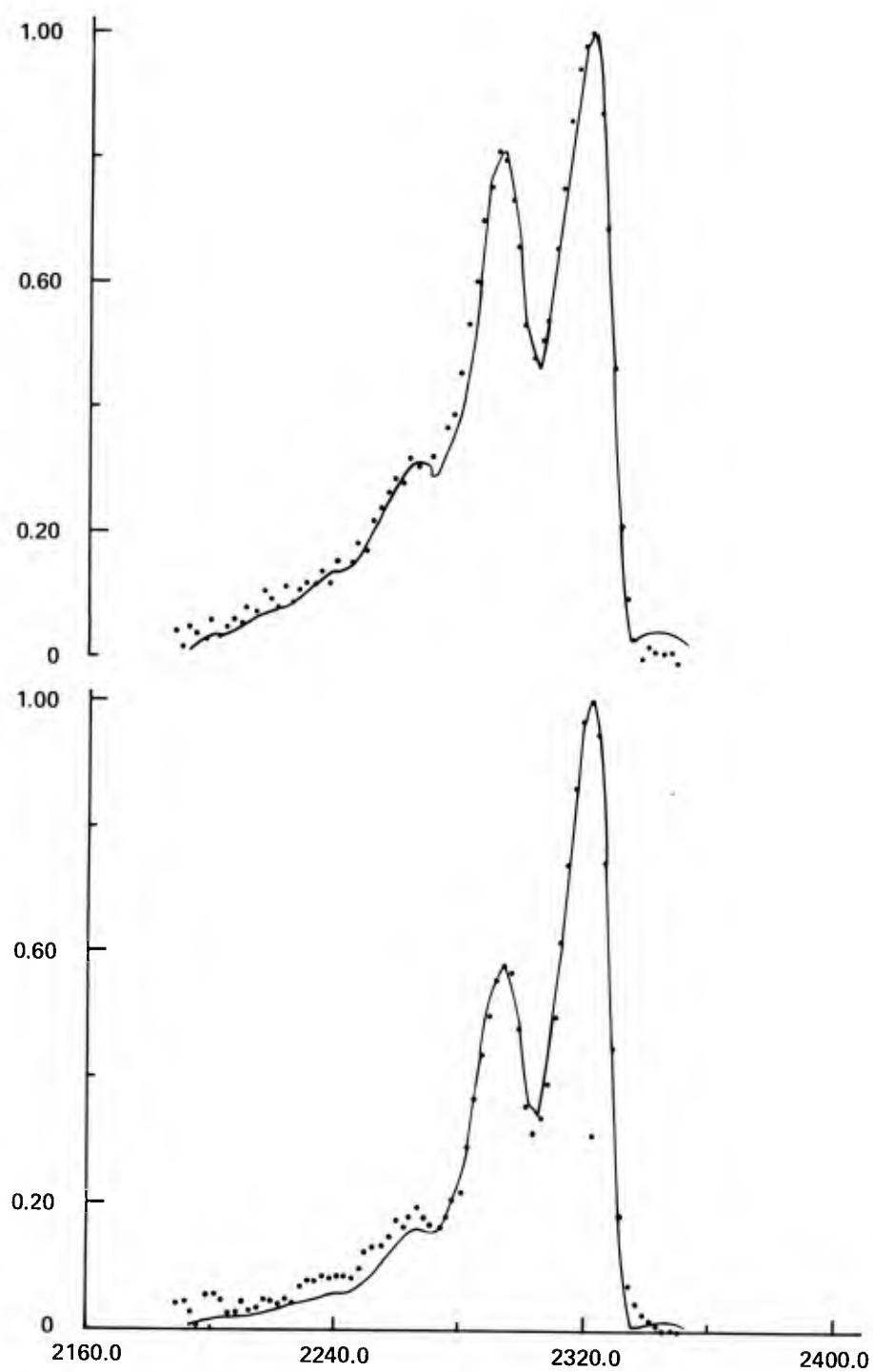


Figure 11. Experimental (•) and calculated  $N_2$  CARS spectra (solid line) 2 mm above the centerline of the burner surface: BOTTOM, 0.4 flame; TOP, 1.0 flame

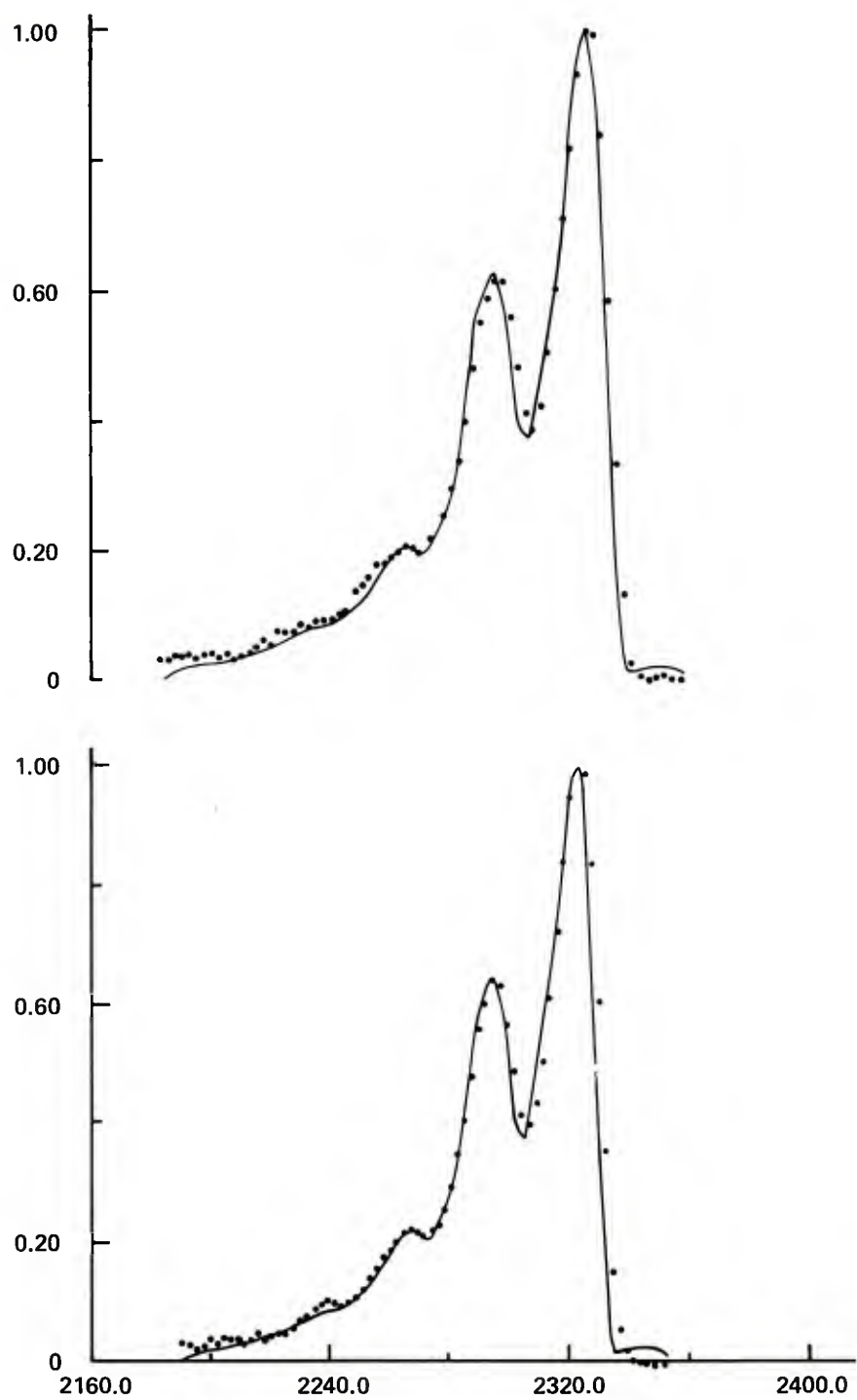


Figure 12. Experimental (•) and calculated  $N_2$  CARS spectra (solid line) from a 0.5 flame at various distances from the burner surface: BOTTOM, 2 mm; TOP, 10 mm

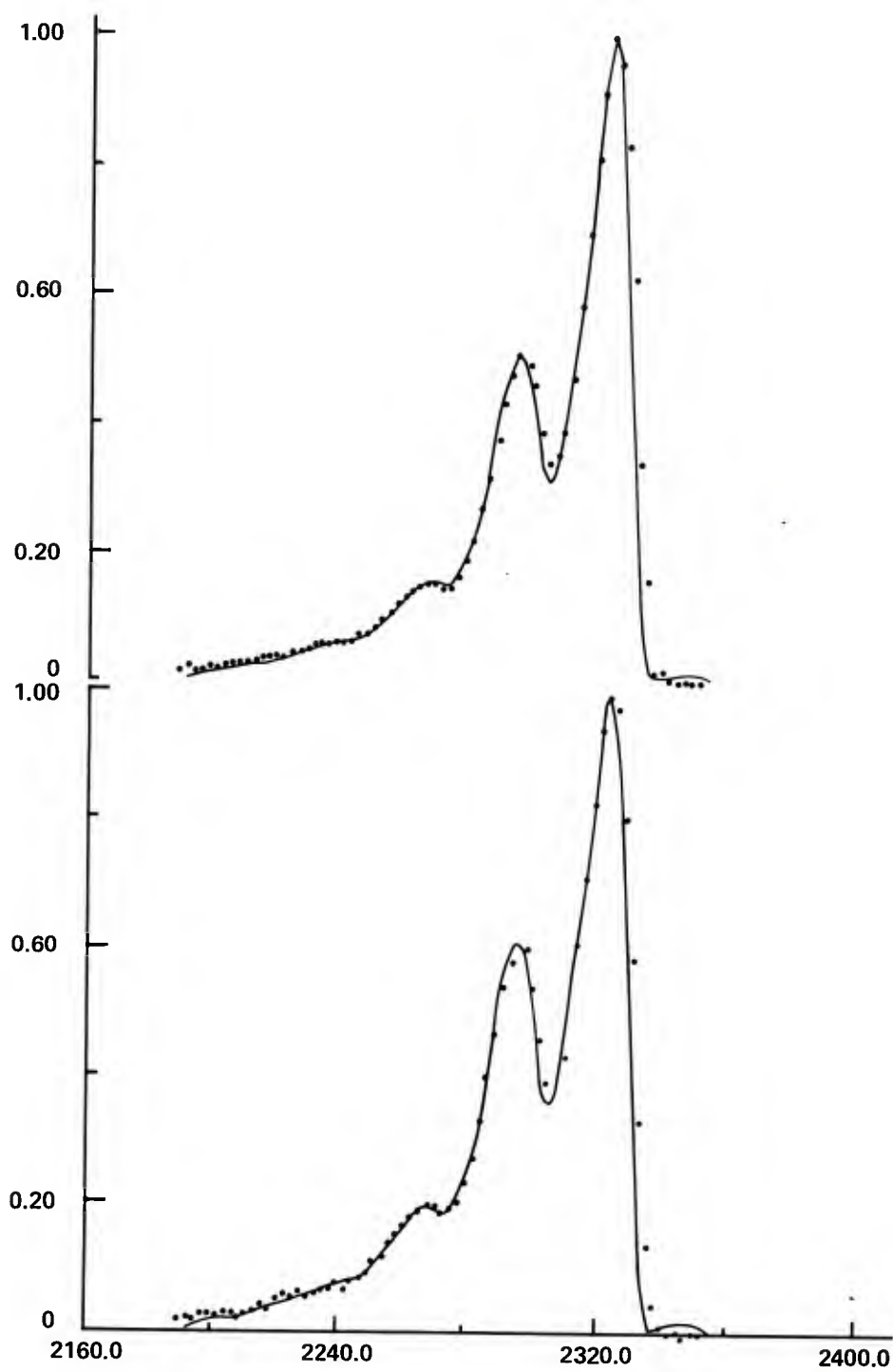


Figure 13. Experimental (•) and calculated  $N_2$  CARS spectra (solid line) from 0.5 flame at various distances from the burner surface: BOTTOM, 20 mm; TOP, 40 mm



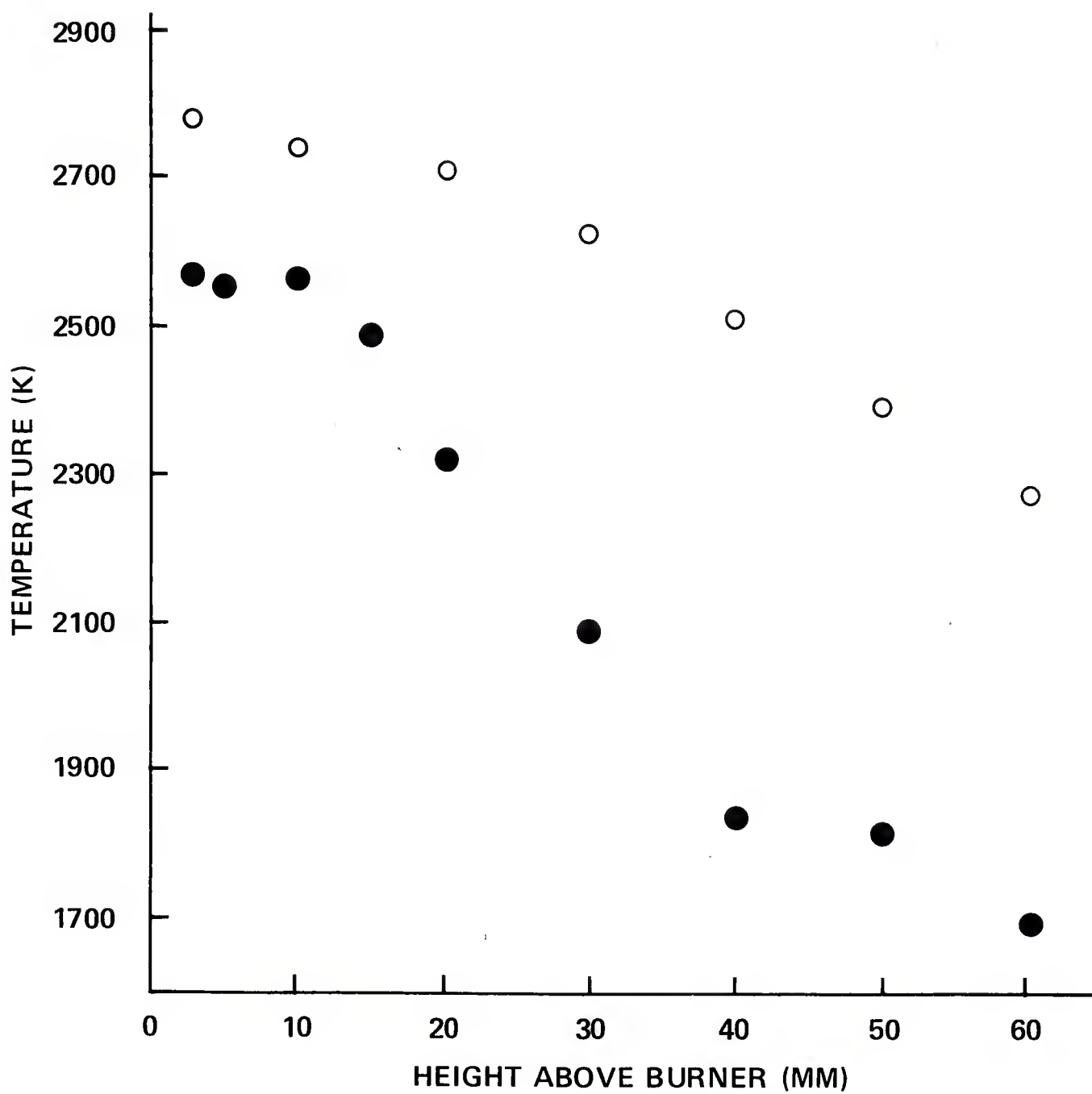


Figure 14. Temperature versus distance above the burner surface for a 0.5 flame at a flow of 16.8 (•) and 33.4 (o) cm/s

DISTRIBUTION LIST

Commander  
U.S. Army Armament Research  
and Development Command  
ATTN: DRDAR-TSS (5)  
DRDAR-GCL  
DRDAR-LC, J. Frasier  
DRDAR-LCA, A. Moss  
DRDAR-LCA-G, J. Lannon  
D. Downs  
L. Harris (10)  
T. Vladimiroff  
A. Beardell  
Y. Carignon  
J. Fendell  
K. Aron  
E. Petro  
DRDAR-LCE, R. Walker  
P. Marinkas  
C. Capellos  
F. Owens

Dover, NJ 07801

Administrator  
Defense Technical Information Center  
ATTN: Accessions Division (12)  
Cameron Station  
Alexandria, VA 22314

Director  
U.S. Army Materiel Systems  
Analysis Activity  
ATTN: DRXSY-MP  
Aberdeen Proving Ground, MD 21005

Commander/Director  
Chemical Systems Laboratory  
U.S. Army Armament Research  
and Development Command  
ATTN: DRDAR-CLJ-L  
DRDAR-CLB-PA  
APG, Edgewood Area, MD 21010

Director  
Ballistics Research Laboratory  
U.S. Army Armament Research  
and Development Command  
ATTN: DRDAR-TSB-S  
DRDAR-BLP, L. Watermier  
A. Barrows  
G. Adams  
R. Fifer  
M. Miller  
T. Coffee  
J. Heimeryl  
C. Nelson  
J. Vanderhoff  
J. Anderson  
Aberdeen Proving Ground, MD 21005

Chief  
Benet Weapons Laboratory, LCWSL  
U.S. Army Armament Research  
and Development Command  
ATTN: DRDAR-LCB-TL  
Watervliet, NY 12189

Commander  
U.S. Army Armament Materiel  
Readiness Command  
ATTN: DRSAR-LEP-L  
Rock Island, IL 61299

Director  
U.S. Army TRADOC Systems  
Analysis Activity  
ATTN: ATAA-SL  
White Sands Missile Range, NM 88002

Director  
Defense Advanced Research Projects  
Agency  
ATTN: LTC C. Buck  
1400 Wilson Boulevard  
Arlington, VA 22209

Director  
Institute for Defense Analyses  
ATTN: H. Wolfhard  
R. T. Oliver  
400 Army-Navy Drive  
Arlington, VA 22202

Commander  
U.S. Army Materiel Development  
and Readiness Command  
ATTN: DRCDMD-ST  
5001 Eisenhower Avenue  
Alexandria, VA 22333

Commander  
U.S. Army Watervliet Arsenal  
ATTN: SARWV-RD, R. Thierry  
Watervliet, NY 12189

Commander  
U.S. Army Aviation Research  
and Development Command  
ATTN: DRSAB-E  
P.O. Box 209  
St. Louis, MO 63166

Director  
U.S. Army Air Mobility Research  
and Development Laboratory  
Ames Research Center  
Moffett Field, CA 94035

Commander  
U.S. Army Communications Research  
and Development Command  
ATTN: DRDCO-PPA-SA  
Fort Monmouth, NJ 07703

Commander  
U.S. Army Electronics Research  
and Development Command  
Technical Support Activity  
ATTN: DELSD-L  
Fort Monmouth, NJ 07703

Commander  
U.S. Army Missile Command  
ATTN: DRSMI-R  
DRSMI-YDL  
Redstone Arsenal, AL 35809

Commander  
U.S. Army Natick Research  
and Development Command  
ATTN: DRXRE, D. Sieling  
Natick, MA 01762

Commander  
U.S. Army Tank Automotive Research  
and Development Command  
ATTN: DRDTA-UL  
Warren, MI 48090

Commander  
U.S. Army White Sands Missile Range  
ATTN: STEWS-VT  
White Sands Missile Range, NM 88002

Commander  
U.S. Army Materials and  
Mechanics Research Center  
ATTN: DRXMR-ATL  
Watertown, MA 02172

Commander  
U.S. Army Research Office  
ATTN: Technical Library  
D. Squire  
F. Schmiedeshaff  
R. Ghirardelli  
M. Ciftan  
P.O. Box 12211  
Research Triangle Park, NC 27706

Office of Naval Research  
ATTN: Code 473  
G. Neece  
800 N. Quincy Street  
Arlington, VA 22217

Commander  
Naval Sea Systems Command  
ATTN: J. W. Murrin, SEA-62R2  
National Center  
Bldg 2, Room 6E08  
Washington, DC 20362

Commander  
Naval Surface Weapons Center  
ATTN: Library Branch, DX-21  
Dahlgren, VA 22448

Commander  
Naval Surface Weapons Center  
ATTN: Code 240, S. J. Jacobs, J. Sharma  
Code 730  
Silver Spring, MD 20910

Commander  
Naval Underwater Systems Center  
Energy Conversion Department  
ATTN: Code 5B331, R. S. Lazar  
Newport, RI 02840

Commander  
Naval Weapons Center  
ATTN: R. Derr  
C. Thelen  
China Lake, CA 93555

Commander  
Naval Research Laboratory  
ATTN: Code 6180  
Washington, DC 20375

Superintendent  
Naval Postgraduate School  
ATTN: Technical Library  
D. Netzer  
A. Fuhs  
Monterey, CA 93940

Commander  
Naval Ordnance Station  
ATTN: Dr. Charles Dale  
Technical Library  
Indian Head, MD 20640

AFOSR  
ATTN: J. F. Masi  
B. T. Wolfson  
D. Ball  
L. Caveny  
Bolling AFB, DC 20332

AFRPL (DYSC)  
ATTN: D. George  
J. N. Levine  
Edwards AFB, CA 93523

National Bureau of Standards  
ATTN: J. Hastie  
T. Kashiwagi  
H. Semerjian  
M. Jacox  
K. Smyth  
J. Stevenson  
Washington, DC 20234

Lockheed Palo Alto Research Laboratories  
ATTN: Technical Information Center  
3521 Hanover Street  
Palo Alto, CA 94304

Aerojet Solid Propulsion Co.  
ATTN: P. Micheli  
Sacramento, CA 95813

ARO Incorporated  
ATTN: N. Dougherty  
Arnold AFS, TN 37389

Atlantic Research Corporation  
ATTN: M. K. King  
5390 Cherokee Avenue  
Alexandria, VA 22314

AVCO Corporation  
AVCO Everett Research Laboratory  
Division  
ATTN: D. Stickler  
2385 Revere Beach Parkway  
Everett, MA 02149

Calspan Corporation  
ATTN: E. B. Fisher  
A. P. Trippe  
P.O. Box 400  
Buffalo, NY 14221

Foster Miller Associates, Inc.  
ATTN: A. J. Erickson  
135 Second Avenue  
Waltham, MA 02154

General Electric Company  
Armament Department  
ATTN: M. J. Bulman  
Lakeside Avenue  
Burlington, VT 05402

General Electric Company  
Flight Propulsion Division  
ATTN: Technical Library  
Cincinnati, OH 45215

Hercules Incorporated  
Allegheny Ballistic Lab  
ATTN: R. Miller  
Technical Library  
Cumberland, MD 21501

Hercules Incorporated  
Bacchus Works  
ATTN: B. Isom  
Magna, UT 84044

IITRI  
ATTN: M. J. Klein  
10 West 35th Street  
Chicago, IL 60615

Olin Corporation  
Badger Army Ammunition Plant  
ATTN: J. Ramnarace  
Baraboo, WI 53913

Olin Corporation  
New Haven Plant  
ATTN: R. L. Cook  
D. W. Riefler  
275 Winchester Avenue  
New Haven, CT 06504

Paul Gough Associates, Inc.  
ATTN: P. S. Gough  
P.O. Box 1614  
Portsmouth, NH 03801

Physics International Company  
2700 Merced Street  
Leandro, CA 94577

Pulsepower Systems, Inc.  
ATTN: L. C. Elmore  
815 American Street  
San Carlos, CA 94070

Rockwell International Corp.  
Rocketdyne Division  
ATTN: C. Obert  
J. E. Flanagan  
A. Axeworthy  
6633 Canoga Avenue  
Canoga Park, CA 91304

Rockwell International Corp.  
Rocketdyne Division  
ATTN: W. Haymes  
Technical Library  
McGregor, TX 76657



Science Applications, Inc.  
ATTN: R. B. Edelman  
Combustion Dynamics and  
Propulsion Division  
23146 Cumorah Crest  
Woodland Hills, CA 91364

Shock Hydrodynamics, Inc.  
ATTN: W. H. Anderson  
4710-16 Vineland Avenue  
N. Hollywood, CA 91602

Thiokol Corporation  
Elkton Division  
ATTN: E. Sutton  
Elkton, MD 21921

Thiokol Corporation  
Huntsville Division  
ATTN: D. Flanigan  
R. Glick  
Technical Library  
Huntsville, AL 35807

Thiokol Corporation  
Wasatch Division  
ATTN: J. Peterson  
Technical Library  
P.O. Box 524  
Brigham City, UT 84302

TRW Systems Group  
ATTN: H. Korman  
One Space Park  
Redondo Beach, CA 90278

United Technologies  
Chemical Systems Division  
ATTN: R. Brown  
Technical Library  
P.O. Box 358  
Sunnyvale, CA 94086

Universal Propulsion Co.  
ATTN: H. J. McSpadden  
1800 W. Deer Valley Road  
Phoenix, AZ 85027

Battelle Memorial Institute  
ATTN: Technical Library  
R. Bartlett  
505 King Avenue  
Columbus, OH 43201

Brigham Young University  
Department of Chemical Engineering  
ATTN: M. W. Beckstead  
Provo, UT 84601

California Institute of Technology  
204 Karmar Lab  
Mail Stop 301-46  
ATTN: F. E. C. Culick  
1201 E. California Street  
Pasadena, CA 91125

Case Western Reserve University  
Division of Aerospace Sciences  
ATTN: J. Tien  
Cleveland, OH 44135

Georgia Institute of Technology  
School of Aerospace Engineering  
ATTN: B. T. Zinn  
E. Price  
W. C. Strahle  
Atlanta, GA 30332

Institute of Gas Technology  
ATTN: D. Gidaspow  
3424 S. State Street  
Chicago, IL 60616

Johns Hopkins University/APL  
Chemical Propulsion Information Agency  
ATTN: T. Christian  
Johns Hopkins Road  
Laurel, MD 20810

Massachusetts Institute of Technology  
Department of Mechanical Engineering  
ATTN: T. Toong  
Cambridge, MA 02139

Pennsylvania State University  
Applied Research Laboratory  
ATTN: G. M. Faeth  
P.O. Box 30  
State College, PA 16801

Pennsylvania State University  
Department of Mechanical Engineering  
ATTN: K. Kuo  
University Park, PA 16801

Pennsylvania State University  
Department of Material Sciences  
ATTN: H. Palmer  
University Park, PA 16801

Princeton Combustion Research  
Laboratories  
ATTN: M. Summerfield  
N. Messina  
1041 U.S. Highway One North  
Princeton, NJ 08540

Princeton University  
Forrestal Campus  
ATTN: I. Glassman  
F. Dryer  
Technical Library  
P.O. Box 710  
Princeton, NJ 08540

Purdue University  
School of Mechanical Engineering  
ATTN: J. Osborn  
S. N. B. Murthy  
N. M. Laurendeau  
TSPC Chaffee Hall  
W. Lafayette, IN 47906

Rutgers State University  
Department of Mechanical and  
Aerospace Engineering  
ATTN: S. Temkin  
University Heights Campus  
New Brunswick, NJ 08903

SRI International  
ATTN: Technical Library  
D. Crosley  
J. Barker  
D. Golden  
333 Ravenswood Avenue  
Menlo Park, CA 94025

Stevens Institute of Technology  
Davidson Library  
ATTN: R. McAlevy, III  
Hoboken, NJ 07030

United Technology  
ATTN: Alan Ecbreth  
Robert Hall  
Research Center  
East Hartford, CT 06108

Commander  
Naval Research Laboratory  
Chemistry Division  
ATTN: A. Harvey  
Washington, DC 20375

General Motors Research Laboratory  
ATTN: J. H. Bechtel  
Warren, Michigan 48090

System Research Laboratory  
ATTN: L. Goss  
2600 Indian Ripple Rd  
Dayton, Ohio 45440

Exxon Research and Engineering  
ATTN: A. Dean  
M. Chou  
P.O. Box 45  
Linden, NJ 07036

Ford Motor Company  
Research Staff  
ATTN: K. Marko  
L. Rimai  
Dearborn, Michigan 48120

Sandia Laboratories  
Applied Physics Division I  
ATTN: L. Rahn  
D. Stephenson  
Livermore, CA 94550

Rensselaer Polytechnic Institute  
Dept. of Chem. Engineering  
ATTN: A. Fontijn  
Troy, NY 12181

University of California,  
San Diego  
Ames Department  
ATTN: F. Williams  
P.O. Box 109  
La Jolla, CA 92037

University of California  
Dept. of Mechanical Eng.  
ATTN: J. W. Daily  
Berkeley, CA 94720

Univ. of Dayton  
University of Dayton Research Inst.  
Dayton, OH 45406

University of Florida  
Dept. of Chemistry  
ATTN: J. Winefordner  
Gainesville, Florida 32601

University of Illinois  
Dept. of Mechanical Eng.  
ATTN: H. Krier  
144 MEB, 1206 W. Green St.  
Urbana, IL 61801

University of Minnesota  
Dept. of Mechanical Eng.  
ATTN: E. Fletcher  
Minneapolis, MN 55455

University of California,  
Santa Barbara  
Quantum Institute  
ATTN: K. Schofield  
M. Steinberg  
Santa Barbara, CA 93106

University of Southern California  
Department of Chemistry  
ATTN: S. Benson  
Los Angeles, CA 90007

Stanford University  
Department of Mech. Eng.  
ATTN: R. Hanson  
Stanford, CA 93106

University of Texas  
Department of Chemistry  
ATTN: W. Gardiner  
H. Schaefer  
Austin, TX 78712

University of Utah  
Dept. of Chemical Engineering  
ATTN: A. Baer  
G. Flandro  
Salt Lake City, UT 84112